Supplementary Information

Flexible Spacer-block Multi-component Copolymerized Donors Enable Resilient Organic Solar Cells with over 40% Crack-onset Strain

Congqi Lin[abc†], Zhenyu Chen[ab†], Ruixiang Peng[ab], Wei Song[ab]*, Jiangwei Gao[ab], Xueliang Yu[ab], Tingting Feng[abc], Yongqi Bai[ab], and Ziyi Ge[ab]**

[a] Zhejiang Engineering Research Center for Energy Optoelectronic Materials and Devices, Ningbo Institute of Materials Technology & Engineering, Chinese Academy of Sciences, Ningbo 315201, P. R. China

[b] Center of Materials Science and Optoelectronics Engineering, University of Chinese Academy of Sciences, Beijing 100049, P. R. China

[c] Faculty of Materials and Chemical Engineering, Ningbo University, Ningbo 315211, P. R. China.

†These authors contributed equally to this work.

*Corresponding authors, E-mail: pengrx@nimte.ac.cn; songwei@nimte.ac.cn; geziyi@nimte.ac.cn.

1.Materials

The indium tin oxide (ITO) glass was purchased from Suzhou Shang yang Solar Technology Co., Ltd. BTP-eC9 was purchased from **Solarmer Energy Inc**, monomers (4, 8-bis (4-chloro-5-(2-ethylhexyl) thiophen-2-yl) benzo [1, 2-b: 4, 5-b'] dithiophene-2, 6-diyl) bis (trimethylstannane); 1, 3-bis (5-bromothiophen-2-yl)-5, 7-bis (2-ethylhexyl)-4H, 8H-benzo [1, 2-c: 4, 5-c'] dithiophene-4, 8-dione; 5, 8-bis(5-bromo-4-(2-butyloctyl) thiophen-2-yl) dithieno [3', 2': 3, 4; 2'', 3'': 5, 6] benzo [1, 2-c] [1, 2, 5] thiadiazole; (3-chlorothiophen-2-yl) trimethylstannane; and 1, 4-bis((5-(trimethylstannyl) thiophen-2-yl) thio) butane were purchased from **Nanjing Zhi yan Technology Co., Ltd**.

The PM6, BTP-eC9, D18, PY-IT, and PDINN were purchased from **Solarmer Materials Inc**. Toluene was purchased from **Zhengzhou Alfa Chemical Co., Ltd.**, chloroform was commercially available from **China National Medicines Corporation Ltd**. PEDOT: PSS (Clevios P VP 4083) was obtained from **J&K Chemicals Inc**. All reagents were directly used without any further treatment, meanwhile, all of reactions were carried out under a nitrogen atmosphere.

2.The synthetic route of MCD PM6-Cl_n-*r*-D18-Cl_{1-n}-TCl (PM6-$Cl_{0.8}$-*r*-D18-$Cl_{0.2}$-TCl (n=0.8)).

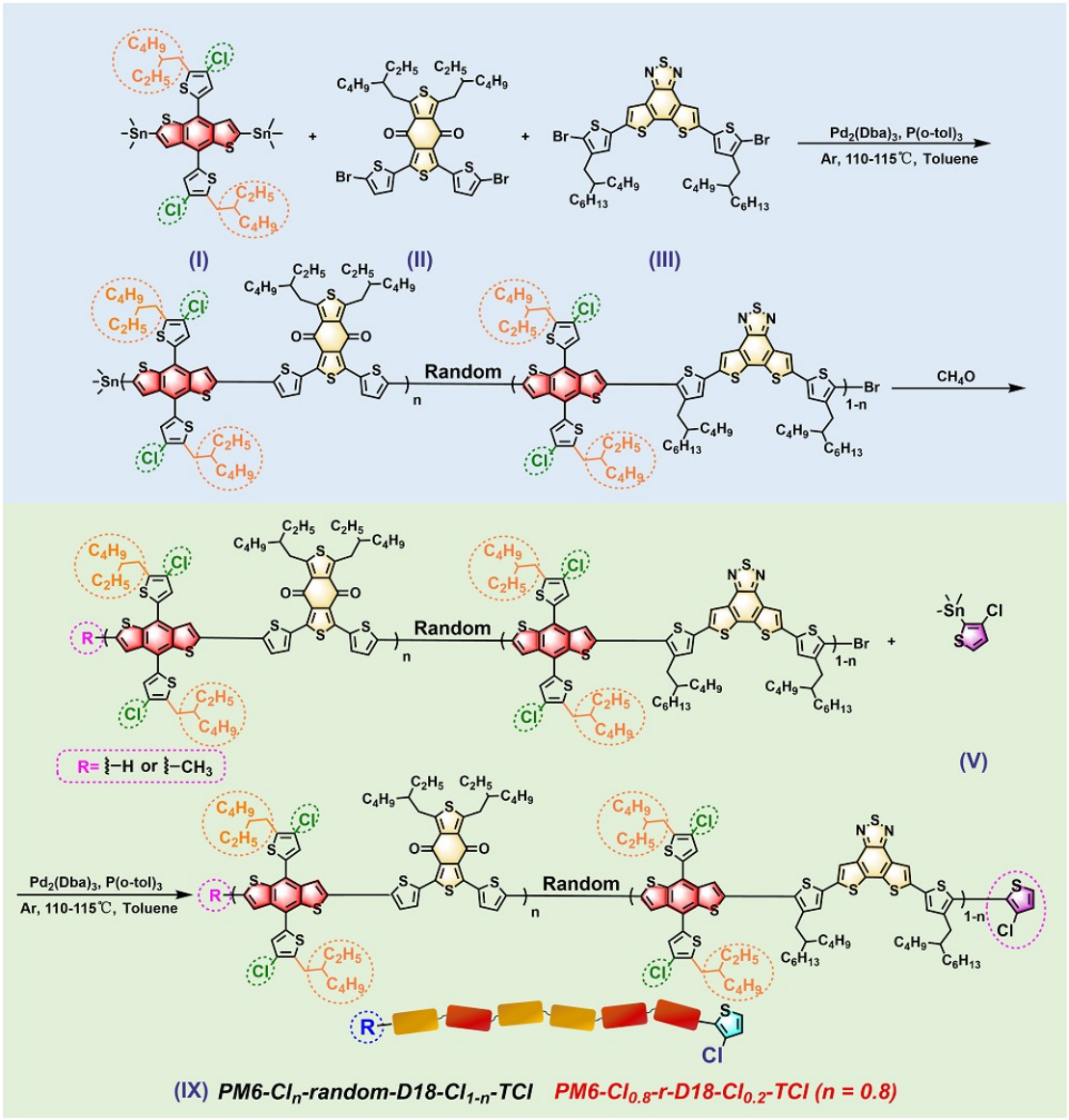

Figure S1. The synthetic route of *random* MCD **PM6-Cl_n-*r*-D18-Cl_{1-n}-TCl**.

2.The synthetic routes of MCDs PM6-Cl_n-*b*-D18-Cl_{1-n}-TCl (PM6-$C1_{0.8}$-*b*-D18-$Cl_{0.2}$-TCl (n=0.8), PM6-$C1_{0.5}$-*b*-D18-$Cl_{0.5}$-TCl (n=0.5), and PM6-$C1_{0.2}$-*b*-D18-$Cl_{0.8}$-TCl (n=0.2)) as well as PM6-Cl_n-*b*-D18-Cl_{1-n}-BTB (PM6-$C1_{0.8}$-*b*-D18-$Cl_{0.2}$-BTB (n=0.8)).

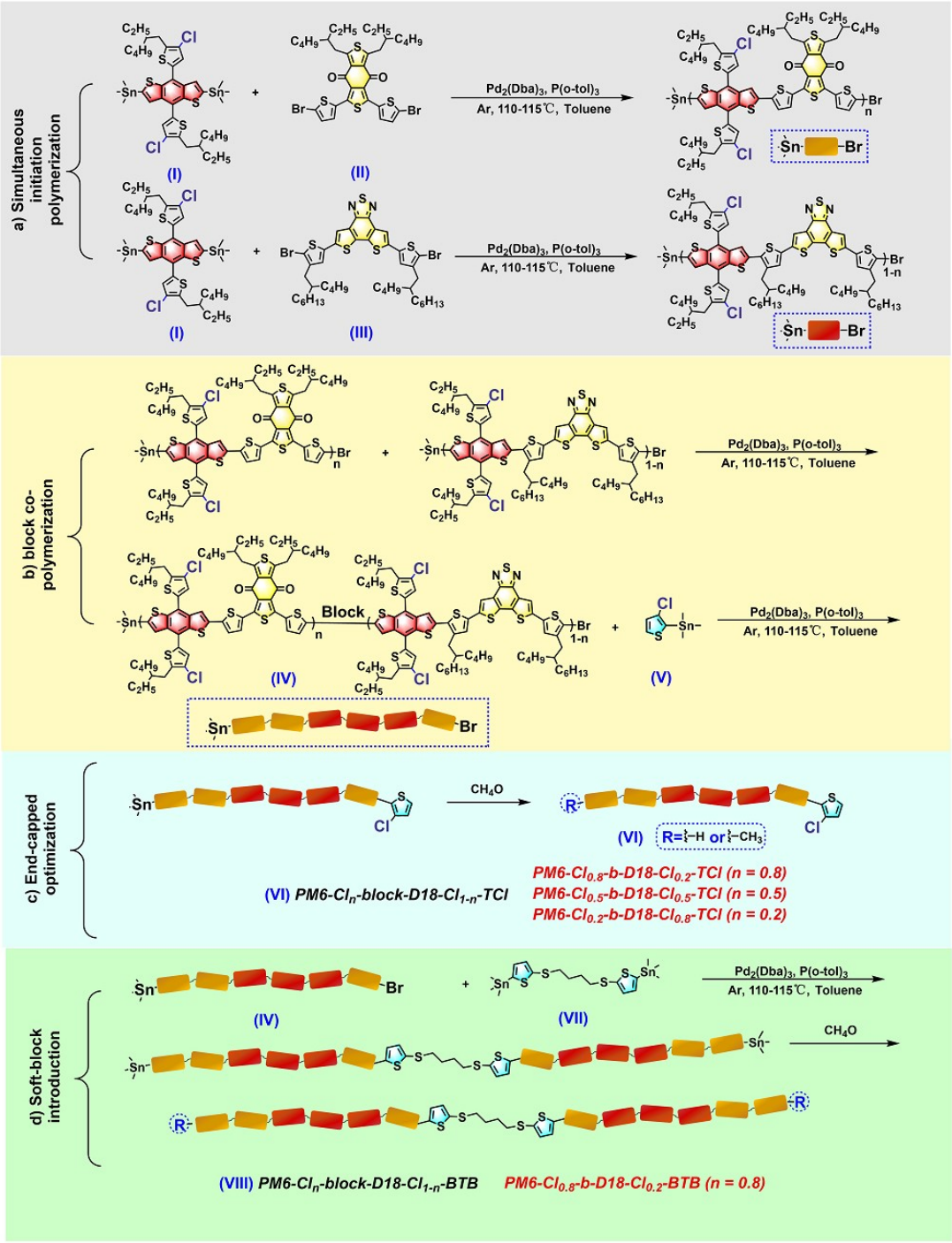

Figure S2. The synthetic route of *sequentially-block* MCD **PM6-Cl_n-*b*-D18-Cl_{1-n}-TCl** and *flexible-spacer block* MCD **PM6-Cl_n-*b*-D18-Cl_{1-n}-BTB**.

Monomer (I): (4, 8-bis (4-chloro-5-(2-ethylhexyl) thiophen-2-yl) benzo [1, 2-*b*: 4, 5-*b*'] dithiophene-2, 6-diyl) bis (trimethylstannane), molecular weight (M_w): 973.45 g mol^{-1}, ^{1}H NMR (400 MHz, $CDCl_3$) δ 7.63 (s, 2H), 7.25 (s, 2H), 2.85 (dd, *J*=7.2, 3.4 Hz, 4H), 1.76 (p, *J*=6.4 Hz, 2H), 1.52–1.33 (m, 16H), 0.99–0.89 (m, 12H), 0.42 (s, 18H).

Monomer (II): 1, 3-bis (5-bromothiophen-2-yl)-5, 7-bis(2-ethylhexyl)-4H, 8H-benzo [1, 2-c: 4, 5-c'] dithiophene-4, 8-dione, M_w: 766.72 g mol^{-1}, ^{1}H NMR (400 MHz, $CDCl_3$) δ 7.44 (d, *J*=4.0 Hz, 2H), 7.06 (d, *J*=4.0 Hz, 2H), 3.30 (t, *J*=7.7 Hz, 4H), 1.80–1.72 (m, 2H), 1.43–1.29 (m, 16H), 0.92 (q, *J*=7.6 Hz, 12H).

Monomer (III): 5, 8-bis (5-bromo-4-(2-butyloctyl) thiophen-2-yl) dithieno [3', 2': 3, 4; 2'', 3'': 5, 6] benzo [1, 2-c] [1, 2, 5] thiadiazole, M_w: 907.02 g mol^{-1}, ^{1}H NMR (400 MHz, $CDCl_3$): δ=7.90 (s, 2H), 6.98 (s, 2H), 2.51 (d, *J* = 7.1, 4H), 1.71-1.99 (s, 2H), 1.39-1.26 (m, 32H), 0.95-0.85 (m, 12H).

Compound (V): (3-chlorothiophen-2-yl) trimethylstannane, M_w: 281.39 g mol^{-1}, ^{1}H NMR (400 MHz, $CDCl_3$) δ 7.16 (d, *J*=3.2 Hz, 2H), 7.05 (d, *J*=3.3 Hz, 2H), 2.79 (d, *J*=6.6 Hz, 4H), 1.74 (t, *J*=3.4 Hz, 4H), 0.36 (s, 18H).

Compound (VII): 1, 4-bis ((5-(trimethylstannyl) thiophen-2-yl) thio) butane, M_w: 612.10 g mol^{-1}, ^{1}H NMR (400 MHz, $CDCl_3$) δ 7.16 (d, *J*=3.2 Hz, 2H), 7.05 (d, *J*=3.3 Hz, 2H), 2.79 (d, *J*=6.6 Hz, 4H), 1.74 (t, *J*=3.4 Hz, 4H), 0.36 (s, 18H).

Synthesis of *random* MCD (IX) PM6-$Cl_{0.8}$-*r*-D18-$Cl_{0.2}$-TCl: **Monomer (I)** (100 mg, 0.1027 mmol), **monomer (II)** (63.01 mg, 0.08218 mmol), **monomer (III)** (18.64 mg, 0.02055 mmol), additive **$Pd_2(Dba)_3$** (10 mg, 0.0109 mmol) and additive **P(o-tol)$_3$** (10 mg, 0.03285 mmol) were dissolved in **toluene** (1 ml) and stirred at 110°C for 10 h under nitrogen atmosphere. The solvent was removed under vacuum after the reaction mixture was cooled to ambient temperature and settled in methanol. Afterward, **PM6-$Cl_{0.8}$-*r*-D18-$Cl_{0.2}$-TCl** was purified through Soxhlet extraction, followed by acetone, methanol,

dichloromethane, chloroform, and chlorobenzene. Finally, the components in chlorobenzene were collected and settled in methanol. The components in chlorobenzene were finally collected and settled in methanol. After overnight drying in a vacuum drying oven, a brownish yellow target product (118.07 mg, 65% yield) was obtained. ^{1}H NMR ($CDCl_3$): δ=7.52 (br, aromatic protons), 7.00 (br, aromatic protons), 2.97 (br, aliphatic protons), 2.33 (br, aliphatic protons), 1.25-0.69 (br, aromatic protons). $\boldsymbol{M_n}$: 76.7 kDa; $\boldsymbol{M_w}$: 175.3 kDa; ***PDI***: 2.29.

Synthesis of *sequentially-block* MCD (VI) PM6-$Cl_{0.8}$-*b*-D18-$Cl_{0.2}$-TCl: **Monomer (I)** (100 mg, 0.1027 mmol), **monomer (II)** (63.01 mg, 0.08218 mmol), **monomer (III)** (18.64 mg, 0.02055 mmol), additive **$Pd_2(Dba)_3$** (10 mg, 0.0109 mmol) and additive **P(o-tol)$_3$** (10 mg, 0.03285 mmol) were dissolved in **toluene** (1 ml) and stirred at 110℃ for 10 h under nitrogen atmosphere. Until the first step of polymerization is completed, further adding **compound (V)** (34.68 mg, 0.1232 mmol) and continue for 12 h. The solvent was removed under vacuum after the reaction mixture was cooled to ambient temperature and settled in methanol. Afterward, **PM6-$Cl_{0.8}$-*b*-D18-$Cl_{0.2}$-TCl** were purified through Soxhlet extraction, followed by acetone, methanol, dichloromethane, chloroform, and chlorobenzene. Finally, the components in chlorobenzene were collected and settled in methanol. After overnight drying in a vacuum drying oven, a brownish yellow target product (144.94 mg, 67% yield) was obtained. ^{1}H NMR ($CDCl_3$): δ=7.52 (br, aromatic protons), 7.00 (br, aromatic protons), 2.98 (br, aliphatic protons), 2.31 (br, aliphatic protons), 1.26-0.70 (br, aromatic protons). $\boldsymbol{M_n}$: 100.4 kDa; $\boldsymbol{M_w}$: 171.9 kDa; ***PDI***: 1.71.

Synthesis of *sequentially-block* MCD (VI) PM6-$Cl_{0.5}$-*b*-D18-$Cl_{0.5}$-TCl: **Monomer (I)** (100 mg, 0.1027 mmol), **monomer (II)** (39.38 mg, 0.05136 mmol), **monomer (III)** (46.59 mg, 0.05136 mmol), additive **$Pd_2(Dba)_3$** (10 mg, 0.0109 mmol) and additive **P(o-tol)$_3$** (10 mg, 0.03285 mmol) were dissolved in **toluene** (1 ml) and stirred at 110℃ for 10 h under nitrogen atmosphere. Until the first step of polymerization is completed, further adding **compound (V)** (34.68 mg, 0.1232 mmol) and continue for 12 h. The

solvent was removed under vacuum after the reaction mixture was cooled to ambient temperature and settled in methanol. Afterward, **PM6-$Cl_{0.5}$-*b*-D18-$Cl_{0.5}$-TCl** were purified through Soxhlet extraction, followed by acetone, methanol, dichloromethane, chloroform, and chlorobenzene. Finally, the components in chlorobenzene were collected and settled in methanol. After overnight drying in a vacuum drying oven, a brownish yellow target product (139.00 mg, 63% yield) was obtained. ^{1}H NMR ($CDCl_3$): δ=7.52 (br, aromatic protons), 7.00 (br, aromatic protons), 3.01 (br, aliphatic protons), 2.33 (br, aliphatic protons), 1.26-0.65 (br, aromatic protons). M_n: 87.9 kDa; M_w: 165.4 kDa; ***PDI***: 1.92.

Synthesis of *sequentially-block* MCD (VI) PM6-$Cl_{0.2}$-*b*-D18-$Cl_{0.8}$-TCl: **Monomer (I)** (100 mg, 0.1027 mmol), **monomer (II)** (15.75 mg, 0.02054 mmol), **monomer (III)** (74.54 mg, 0.08218 mmol), additive **$Pd_2(Dba)_3$** (10 mg, 0.0109 mmol) and additive **P(o-tol)$_3$** (10 mg, 0.03285 mmol) were dissolved in **toluene** (1 ml) and stirred at 110℃ for 10 h under nitrogen atmosphere. Until the first step of polymerization is completed, further adding **compound (V)** (34.68 mg, 0.1232 mmol) and continue for 12 h. The solvent was removed under vacuum after the reaction mixture was cooled to ambient temperature and settled in methanol. Afterward, **PM6-$Cl_{0.2}$-*b*-D18-$Cl_{0.8}$-TCl** were purified through Soxhlet extraction, followed by acetone, methanol, dichloromethane, chloroform, and chlorobenzene. Finally, the components in chlorobenzene were collected and settled in methanol. After overnight drying in a vacuum drying oven, a brownish yellow target product (134.98 mg, 60% yield) was obtained. ^{1}H NMR ($CDCl_3$): δ=7.52 (br, aromatic protons), 7.00 (br, aromatic protons), 3.00 (br, aliphatic protons), 2.38 (br, aliphatic protons), 1.26-0.66 (br, aromatic protons). M_n: 65.1 kDa; M_w: 154.9 kDa; ***PDI***: 2.38.

Synthesis of *flexible-spacer block* MCD (VIII) PM6-$Cl_{0.8}$-*b*-D18-$Cl_{0.2}$-BTB: **Monomer (I)** (100 mg, 0.1027 mmol), **monomer (II)** (63.01 mg, 0.08218 mmol), **monomer (III)** (18.64 mg, 0.02055 mmol), additive **$Pd_2(Dba)_3$** (10 mg, 0.0109 mmol)

and additive **P(o-tol)$_3$** (10 mg, 0.03285 mmol) were dissolved in **toluene** (1 ml) and stirred at 110℃ for 10 h under nitrogen atmosphere. Until the first step of polymerization is completed, further adding **compound (VII)** (75.46 mg, 0.1232 mmol) and continue for 12 h. The solvent was removed under vacuum after the reaction mixture was cooled to ambient temperature and settled in methanol. Afterward, **PM6-Cl$_{0.8}$-*b*-D18-Cl$_{0.2}$-BTB** were purified through Soxhlet extraction, followed by acetone, methanol, dichloromethane, chloroform, and chlorobenzene. Finally, the components in chlorobenzene were collected and settled in methanol. After overnight drying in a vacuum drying oven, a brownish yellow target product (151.69 mg, 59% yield) was obtained. ^{1}H NMR ($CDCl_3$): δ=7.52 (br, aromatic protons), 7.00 (br, aromatic protons), 2.98 (br, aliphatic protons), 1.26-0.63 (br, aromatic protons). M_n: 93.4 kDa; M_w: 174.0 kDa; ***PDI***: 1.86.

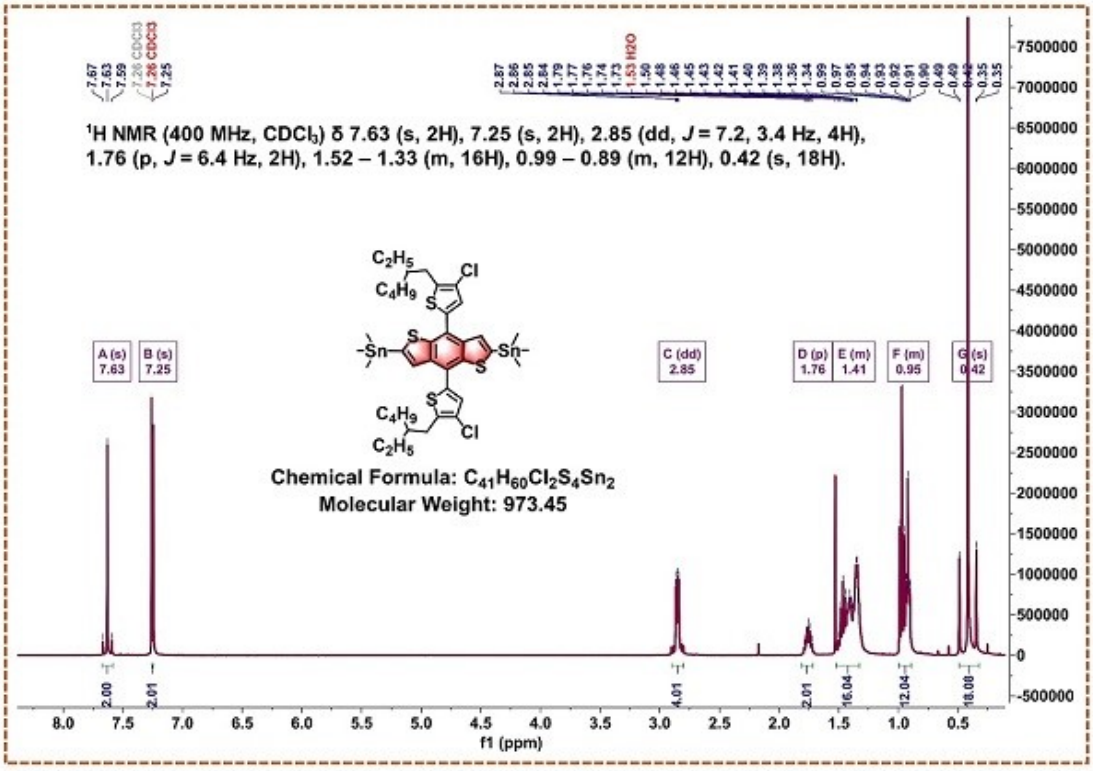

Figure S3. ^{1}H-NMR spectrum of **monomer (I)** in chloroform-*d*.

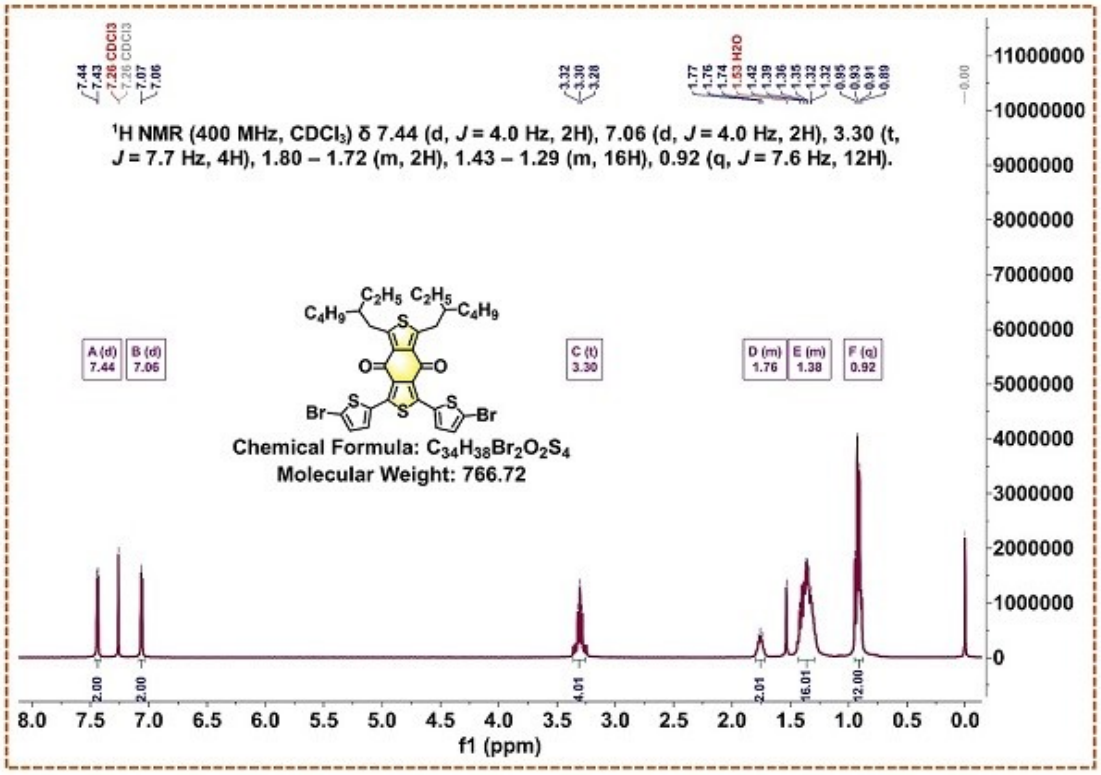

Figure S4. [1]H-NMR spectrum of **monomer (II)** in chloroform-*d*.

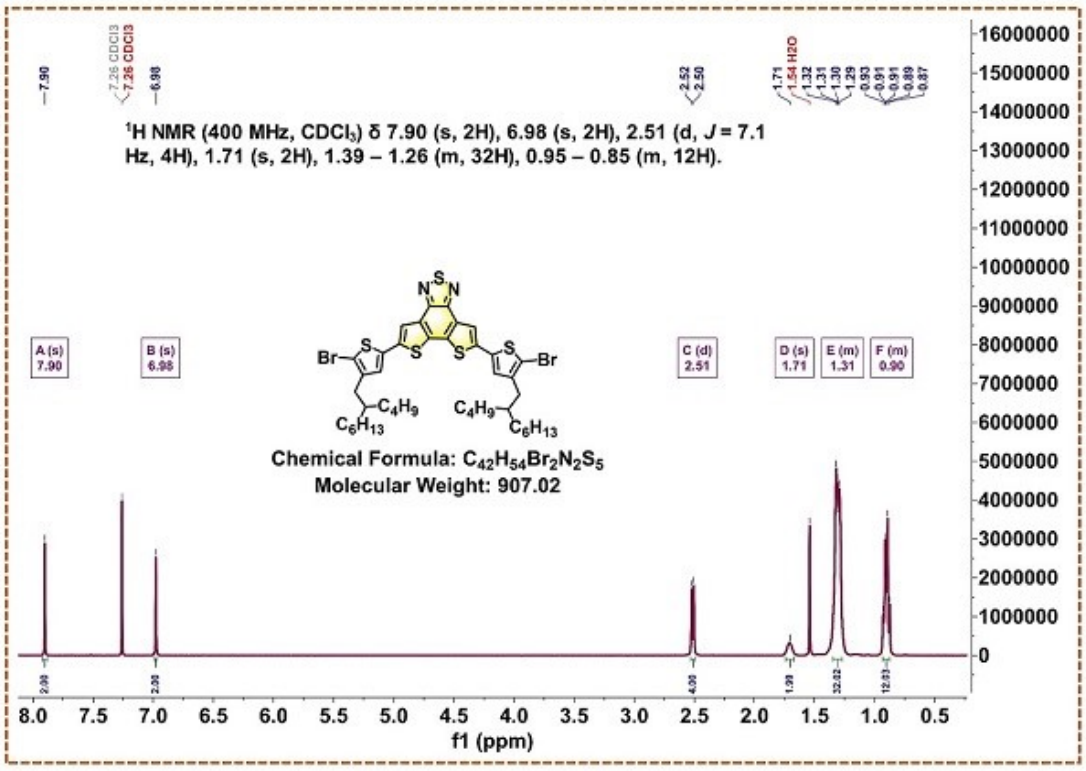

Figure S5. [1]H-NMR spectrum of **monomer (III)** in chloroform-*d*.

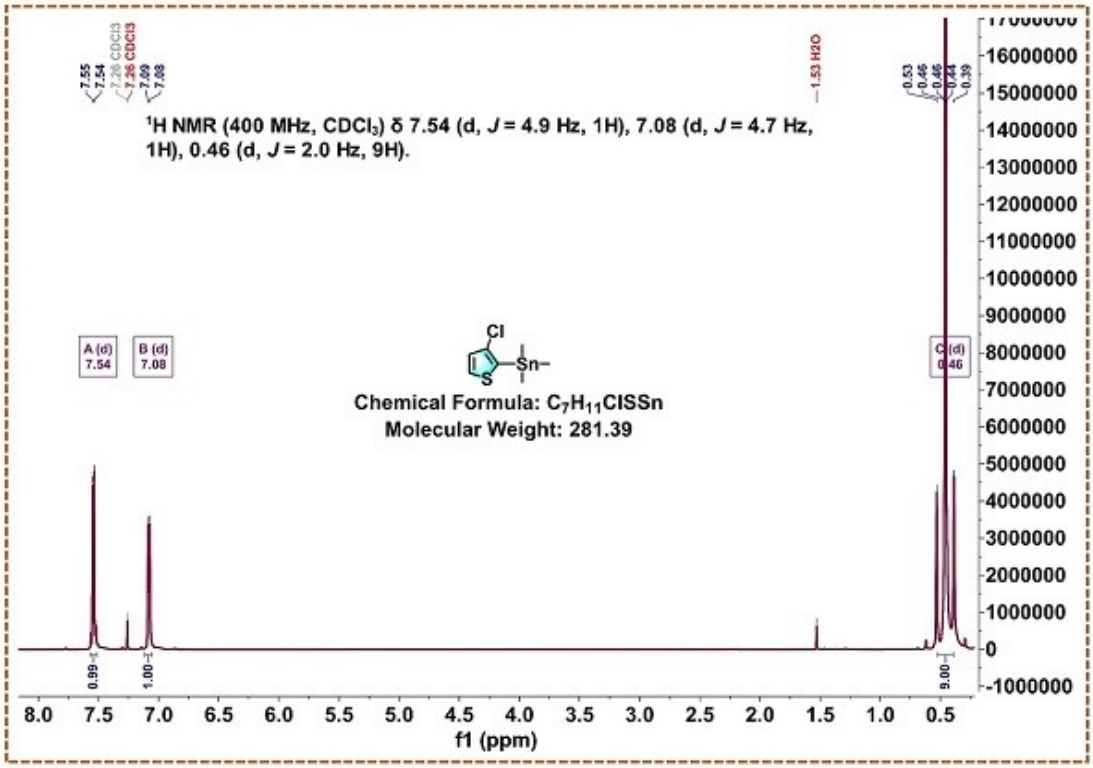

Figure S6. ^{1}H-NMR spectrum of **compound (V)** in chloroform-*d*.

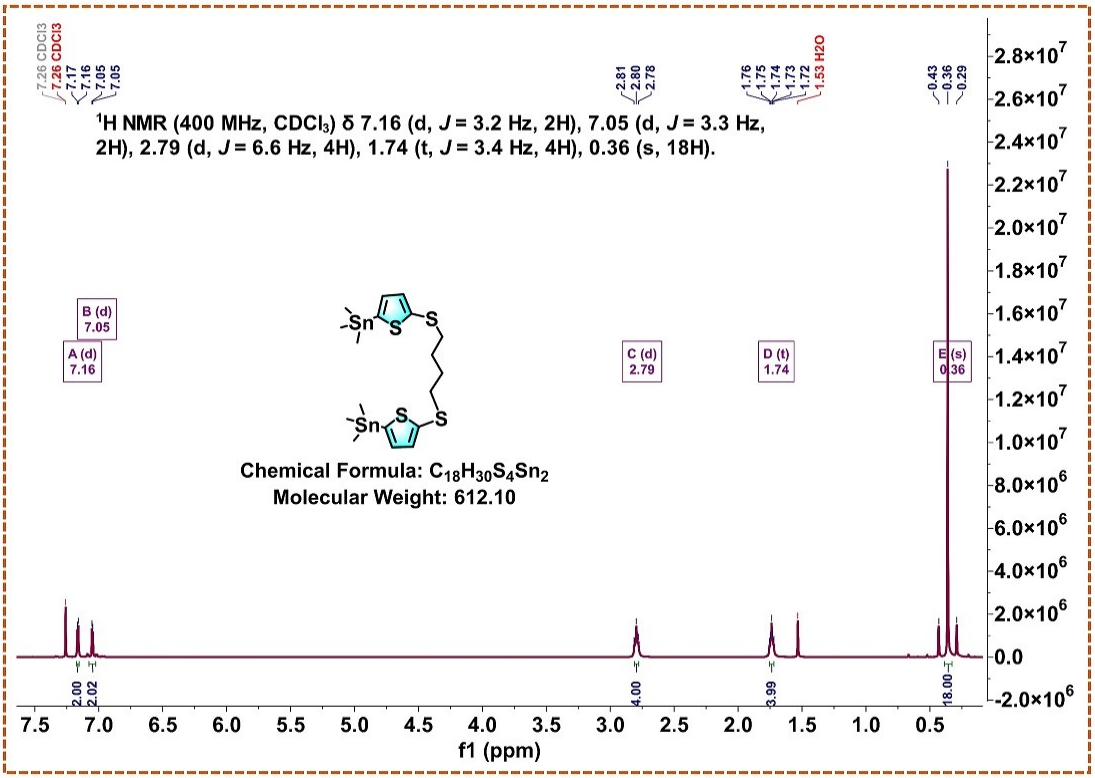

Figure S7. ^{1}H-NMR spectrum of **compound (VII)** in chloroform-*d*.

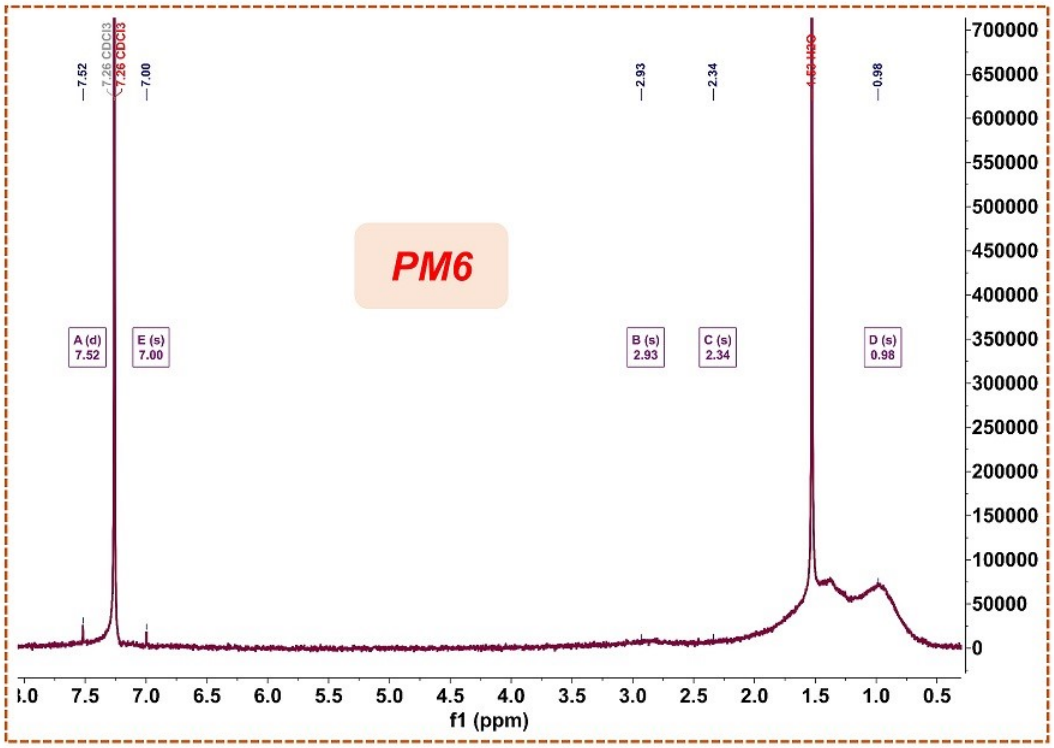

Figure S8. [1]H-NMR spectrum of **PM6** in chloroform-*d*.

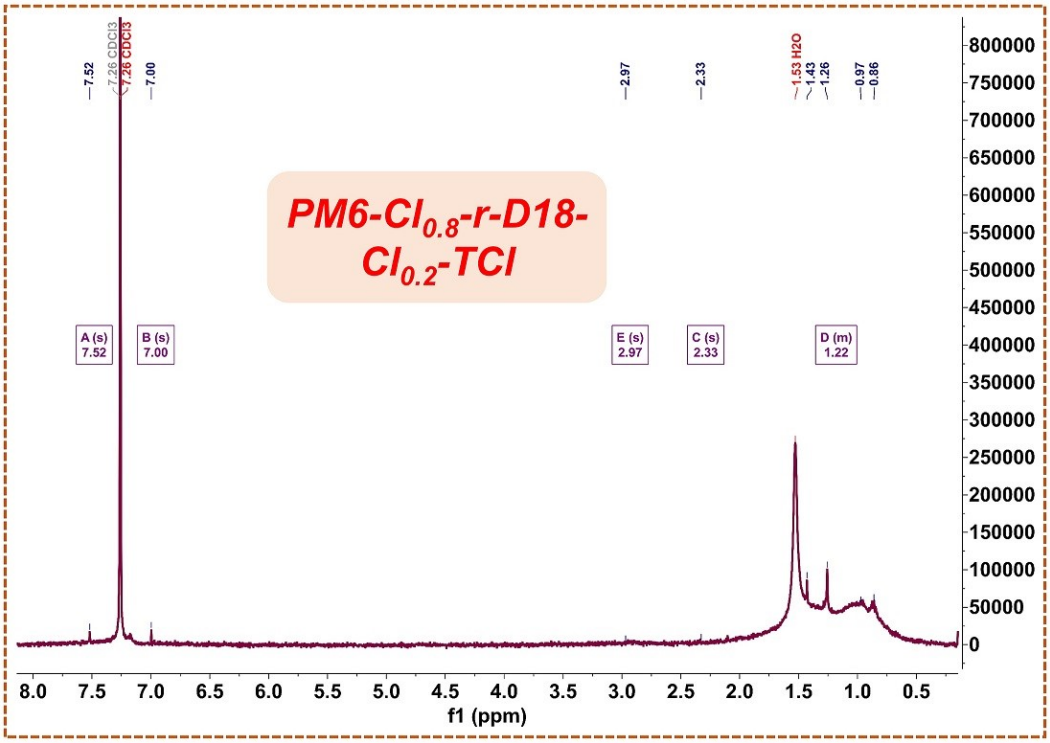

Figure S9. [1]H-NMR spectrum of ***random*** **MCD (IX) PM6-$Cl_{0.8}$-*r*-D18-$Cl_{0.2}$-TCl** in chloroform-*d*.

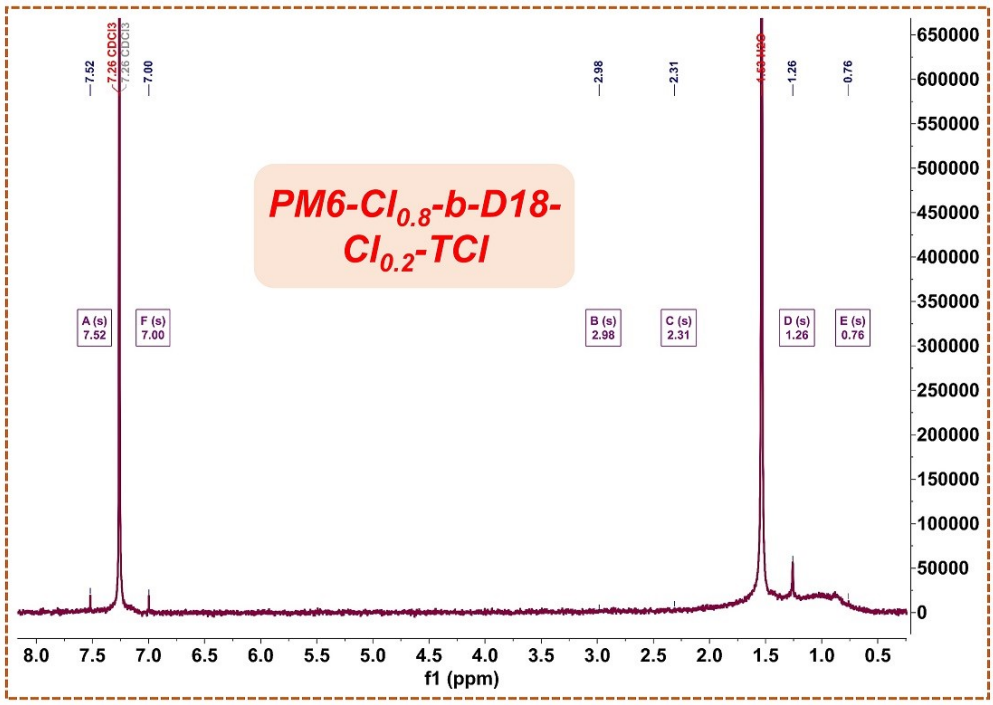

Figure S10. ^{1}H-NMR spectrum of ***sequentially-block*** **MCD (VI) PM6-$Cl_{0.8}$-*b*-D18-$Cl_{0.2}$-TCl** in chloroform-*d*.

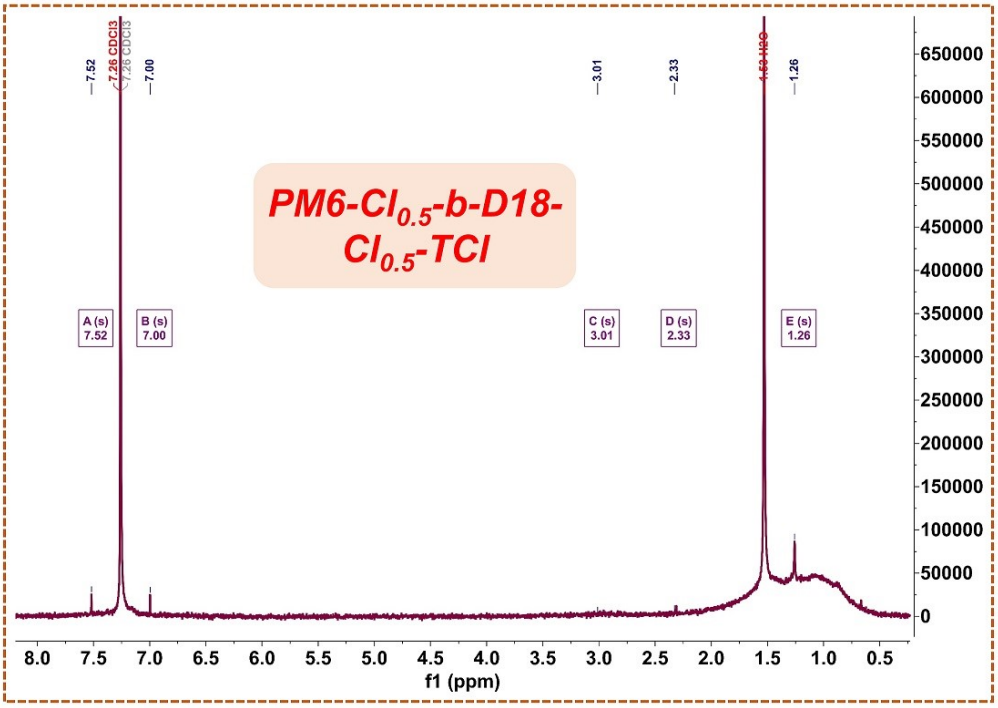

Figure S11. ^{1}H-NMR spectrum of ***sequentially-block*** **MCD (VI) PM6-$Cl_{0.5}$-*b*-D18-$Cl_{0.5}$-TCl** in chloroform-*d*.

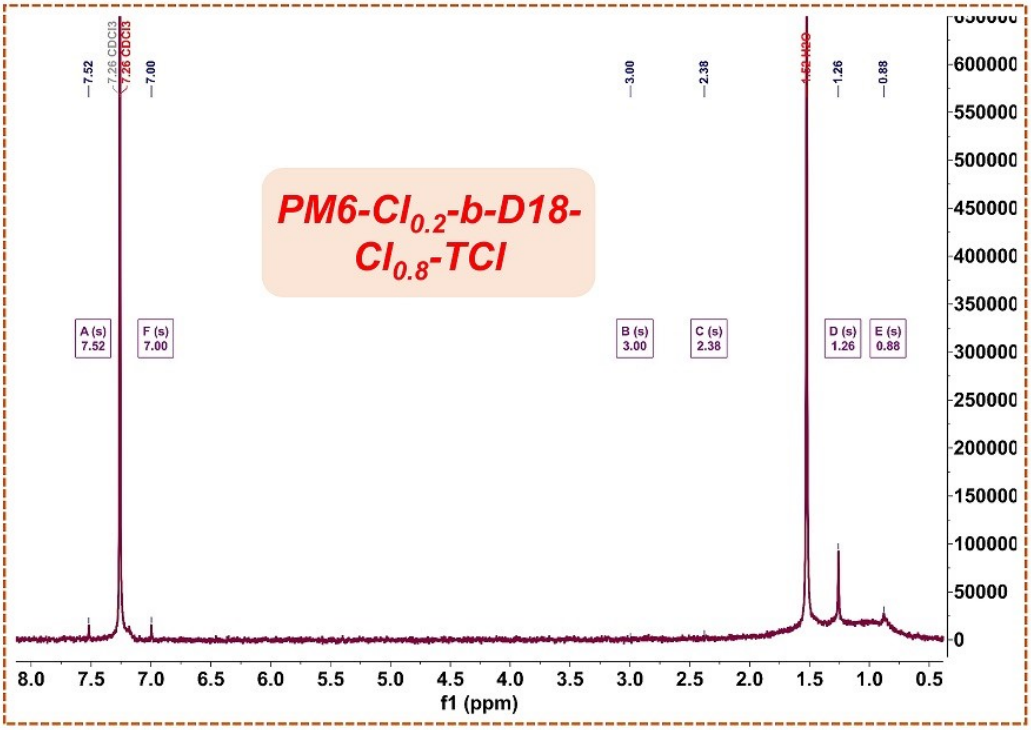

Figure S12. ^{1}H-NMR spectrum of ***sequentially-block*** **MCD (VI) PM6-$Cl_{0.2}$-*b*-D18-$Cl_{0.8}$-TCl** in chloroform-*d*.

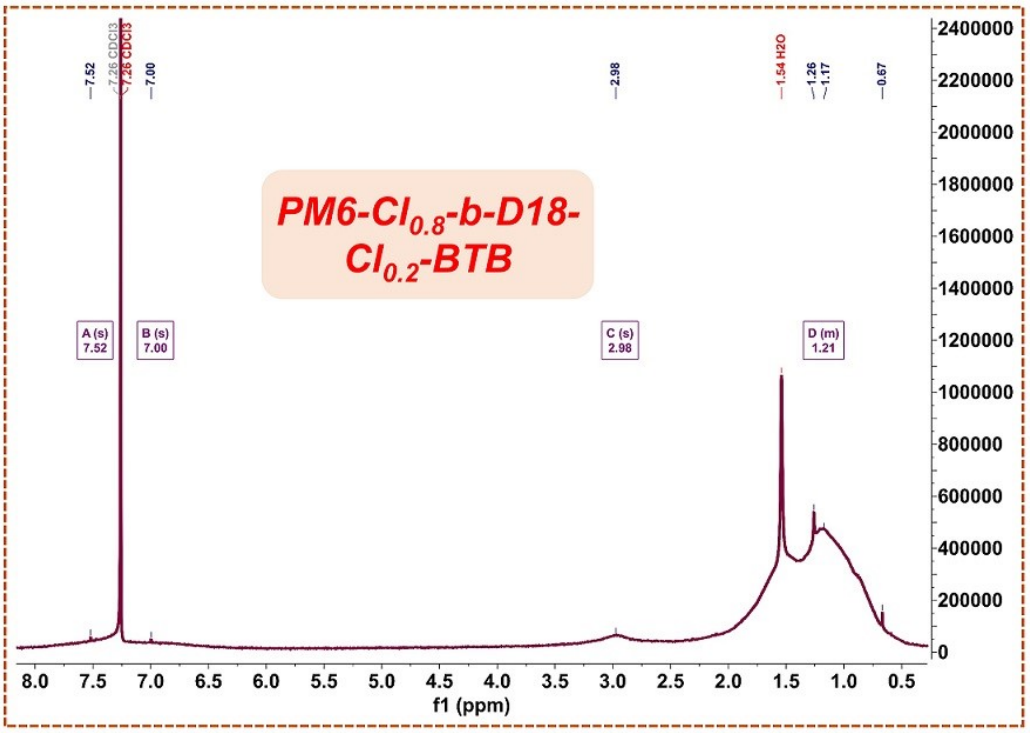

Figure S13. ^{1}H-NMR spectrum of ***flexible-spacer block*** **MCD (VIII) PM6-$Cl_{0.8}$-*b*-D18-$Cl_{0.2}$-BTB** in chloroform-*d*.

3. Measurements and Instruments

Rigid device fabrication and measurement：

The rigid binary OSCs based on **PM6**, **PM6-$Cl_{0.8}$-*r*-D18-$Cl_{0.2}$-TCl**, **PM6-$Cl_{0.8}$-*b*-D18-$Cl_{0.2}$-TCl**, **PM6-$Cl_{0.5}$-*b*-D18-$Cl_{0.5}$-TCl**, **PM6-$Cl_{0.2}$-*b*-D18-$Cl_{0.8}$-TCl**, **PM6-$Cl_{0.8}$-*b*-D18-$Cl_{0.2}$-BTB**, and **PM6-$Cl_{0.8}$-*b*-D18-$Cl_{0.2}$-TCl: PM6 (0.1: 0.9)** were fabricated employing the conventional architecture of ITO/4PADCB or Poly(3,4-ethylenedioxythiophene):polystyrene sulfonate (PEDOT: PSS) 4083/MCD: BTP-eC9 (1.0: 1.2, w/w)/perylene-diimide (PDINN)/Ag. The ITO glass was cleaned with deionized water, acetone and isopropanol in sequence, then treated with the UV-Ozone for 15 minutes. The 4PADCB or PEDOT: PSS 4083 solution was spin-coated at 3000 rpm onto the ITO substrates for 30 seconds. Then the 4PADCB film was heated at 100 ℃ in air for 10 min. The MCD and Y6 were dissolved in solution, the concentration of MCDs in chloroform (CF) solvent was 5.6 mg ml^{-1}, with the solution additive **diiodooctane (DIO)** of 0.3 %. Meanwhile, the solution need be stirred at 45 ˚C at least 4 h to fully dissolve the donor. Then the solution was spin-coated with a speed of 4000 r min^{-1} on the PEDOT: PSS 4083 layer and treated with 95℃ thermal annealing for 10 minutes. With the PDINN (1 mg ml^{-1}, 2000 r min^{-1}) spin-coated on the active layer, the devices were finally transferred to the evaporation tank to deposit Ag of 160 nm. *J-V* measurements of devices were carried out in the **Keithley 2440 source meter** with a solar simulator (**Newport-Oriel® Sol3A 450W**) device. EQE measurements were conducted with the solar cell QE tester (**QE-R, Enli Technology Co., Ltd**).

Flexible OSCs fabrication:

The structure of the flexible device was PEN/ITO/4PADCB/active layer/PDINN/Ag. The PEN/ITO first was adhered onto polydimethylsiloxane (PDMS)-coated glass substrates. The preparation conditions for the 4PADCB and active layer are the same as those for the rigid device. Subsequently, PDINN spin-coated at 2000 rpm for 30 s. Finally, Ag was thermally deposited as an electrode.

Cyclic Voltammetry (CV)

The energy levels for **PM6**, **PM6-$Cl_{0.8}$-*r*-D18-$Cl_{0.2}$-TCl**, **PM6-$Cl_{0.8}$-*b*-D18-$Cl_{0.2}$-TCl**, **PM6-$Cl_{0.5}$-*b*-D18-$Cl_{0.5}$-TCl**, **PM6-$Cl_{0.2}$-*b*-D18-$Cl_{0.8}$-TCl**, and **PM6-$Cl_{0.8}$-*b*-D18-$Cl_{0.2}$-BTB**, were measured by cyclic voltammetry (CV), which was performed by using Ag/AgCl as reference electrode in $C_{16}H_{36}NPF_6$ solution, and ferrocene/ferrocenium (Fc/Fc^+) was used as internal reference. The *HOMO* and *LUMO* energy levels were calculated according to the following equation:

$$\text{HOMO/LUMO} = -(\varphi_{ox/red} - \varphi_{Fc/Fc^+} + 4.8)\ \text{eV}$$

Where φ_{OX} is the onset of oxidation and the φ_{red} relates to the reduction potential, respectively.

Elemental analysis characterization

The mass ratio of elementals Carbon (**C**), nitrogen (**N**), sulfur (**S**), and hydrogen (**H**) were test by **vario ELCUBE**, meanwhile, the mass of each test sample is around 5mg.

GPC characterization

The number-average molecular weight (M_n), M_w and polydispersity index (*PDI*) were acquired on **PL-GPC 220** in 1, 2, 4-trichlorobenzene at 150 ℃, with the flow rate of 1ml min^{-1}. The data detection results and reports are provided by **Shanghai Fuda Testing Technology Group Co., Ltd**.

AFM PFQNM

The DMT modulus, adhesion, deformation, and AFM images were obtained from peak force quantitation nanomechanical mapping (PFQNM) and tapping mode by a **Veeco Dimension 3100V atomic force microscope**.

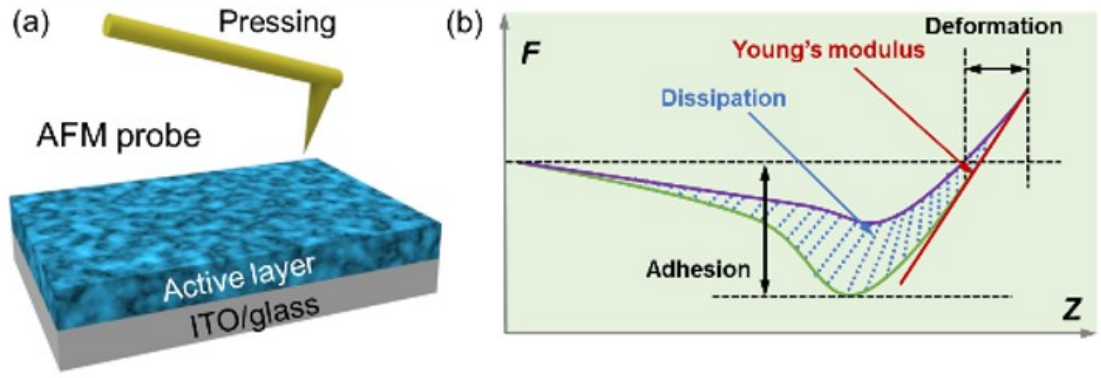

Figure S14. (a) Schematic diagram of the AFM PFQNM technology. (b) Schematic diagram of a full force-distance curve. The Young's modulus can be extracted by extrapolating the linear portion of the retraction curve after the contact point. The adhesion is the vertical distance between the base line and the bottom most part of the retraction curve.

Pseudo free-standing tensile test

Stress-strain curves were tested on in-situ micro-mechanical testing system (**PR-MMT6SL-100F**, **Shenzhen HuaJason Technologies, Co., LTD.**). The films (5.6 mg ml^{-1}) were spin-casted (3000 rms, 30 s) onto the PEDOT: PSS 4083-coated glass substrate at first, and then cut into long strips approximately 5 mm wide and 20 mm long to assemble the sample. Afterward, the films were floated onto the water surface, and attached to the grips by van der Waals forces. The strain was applied at a fixed strain rate, and the tensile load values were measured by a load cell with high resolution, meanwhile; corresponding characterization results were calculated with the film thickness of 100 nm.

Ultraviolet-Visible-Near Infrared (UV-Vis-NIR)

Ultraviolet-Visible-Near Infrared (UV-Vis-NIR) absorption spectra were acquired on a **Perkin-Elmer Lambda 950 spectrophotometer**.

***In-situ* absorption spectra**

In-situ UV-vis absorption measurements were performed by the Filmetrics F20-EXR spectrometer using the transmission mode with a time resolution of 0.025 s. The spectrometer consists of a light source and detector. The light source and detector are fixed above and below the substrate, respectively, and on the same vertical line. The solution was injected into the slot, and the film was coated onto the glass substrate. The detector collects the transmission spectra ranging from 400 to 1050 nm during coating. The UV-vis absorption spectra are calculated from the transmission spectra according to the equation $A_\lambda = - \log_{10}(T)$, where A_λ is the absorbance at a certain wavelength (λ), and T is the calculated transmittance. The light source and detector were turned on before coating the film, so time zero is the point when the first solution transmission spectrum was collected by the detector. Before time zero, there is only noise in the transmission spectra.

The authors thank Dr. Bin Hu (Xi'an Jiaotong University) for assistance with data acquisition.

***In-situ* photoluminescence (PL) spectra**

In-situ Photoluminescence Spectra Measurements were performed by a laser device (**MGL-III-785-300mW BH81223**) with a time resolution of 0.025 s.

Femtosecond transient absorption (fs-TA)

The ultrafast fs-TA measurements were conducted on a fs pump-probe system in association with an amplified laser system under ambient conditions, which consist of a modelocked Ti:sapphire seed laser (**Spectra Physics, Maitai**) directed to a regenerative amplifier (**Spitfire Pro, Spectra Physics**) and a high power laser

(**Empower, Spectra Physics**) used for pumping and amplifier. The amplified 800 nm output was divided into two parts, and the pump pulses with tunable wavelength were generated by the major part of the beam (~85%) after an optical parametric amplifier (**TOPAS prime, Spectra Physics**), while the white-light continuum (**WLC**) probe and reference pulses (420−780 nm) were generated by the rest part of the beam passed through an optical delay line, here, the probe beam traveled through the sample and the reference beam was sent directly to the reference spectrometer. A chopper which can modulate the pump pulses was employed to obtain fs-TA spectra with and without the pump pulses alternately, and an optics fiber coupled to a multichannel spectrometer with a CMOS sensor was used to record the pump-induced fluctuation in probe/reference beam intensity with adjusting the optical delay line (maximum ~3ns). The spectral profiles were further processed by the **Surface Xplorer**.

Space charge limited current (SCLC) method

Electron-only devices were fabricated using the structure of ITO/Ag/active layers/PDINN/Ag. Firstly, after being cleaned with deionized water, acetone and isopropanol, the all-ITO glass was deposited with 100 nm Ag and then the ternary polymer donors and acceptor were spin-coated on the Ag layer and treated with 100 ℃ for 10 minutes. With the PDINN spin-coated on the active layer, the devices were finally transferred to the evaporation tank to deposit 160 nm Ag.

Hole-only devices were fabricated with the structure of ITO/PEDOT: PSS 4083/active layers/MoO_3/Ag. After being cleaned with deionized water, acetone and isopropanol, the all-ITO glass was treated with the UV-Ozone for 15 minutes. The PEDOT: PSS 4083 solution was spin-coated at 3000 rpm onto the ITO substrates for 30 seconds. Then the PEDOT: PSS 4083 film was heated at 150 ℃ for 10 min in atmosphere. Then the donor and acceptor were spin-coated on the PEDOT: PSS 4083 layer and treated with 95 ℃ for 10 minutes. Then devices were finally transferred to the evaporation tank to deposit 10 nm MoO_3 and then 160 nm Ag.

The mobilities were obtained by taking current-voltage curves and fitting the results to a space charge limited form, where the SCLC is described by:

$$J = \frac{9\varepsilon_0\varepsilon_R\mu V^2}{8L^3}$$

Where ε_0 is the permittivity of free space (8.854×10^{-12} F m^{-1}), ε_R is the relative permittivity of the material (assumed to be 3), μ is the electron or hole mobility and L is the thickness of the film. From the plots of $J^{1/2}$ vs V, electron or hole mobilities can be deduced.

Morphology Characterization

AFM height and phase images were measured by **Bruker Dimension ICON** to explore the characteristic of morphology. GIWAXS measurements were performed on a XEUSS SAXS/WAXS system (**Xeuss 3.0**) at the Suzhou institute of Nano-Tech and Nano-Bionics (**SINANO**).

Contact angle measurement

Contact angles were measured from spin-coated films by an optical contact angle meter (CAM 200). The surface energy was estimated by the Harmonic mean equations:

$$(1 + \cos\theta_1)\gamma_1 = 2(\gamma_1^d\gamma_s^d)^{\frac{1}{2}} + 2(\gamma_1^p\gamma_s^p)^{\frac{1}{2}}$$

$$(1 + \cos\theta_2)\gamma_2 = 2(\gamma_2^d\gamma_s^d)^{\frac{1}{2}} + 2(\gamma_2^p\gamma_s^p)^{\frac{1}{2}}$$

$$\gamma_s = \gamma_s^d + \gamma_s^p$$

where γ_s^d represents the dispersive components, γ_s^p is the polar component, γ_s is the surface energy. θ_1 and θ_2 are the contact angles of pure water and glycerol, respectively.

H_2O: γ_1 = 72.8 mJ/m^2, γ_1^d = 21.8 mJ/m^2, γ_1^p=51.0 mJ/m^2.

Diiodomethane: γ_2 = 50.8 mJ/m^2, γ_2^d =48.5 mJ/m^2, γ_2^p=2.3 mJ/m^2.

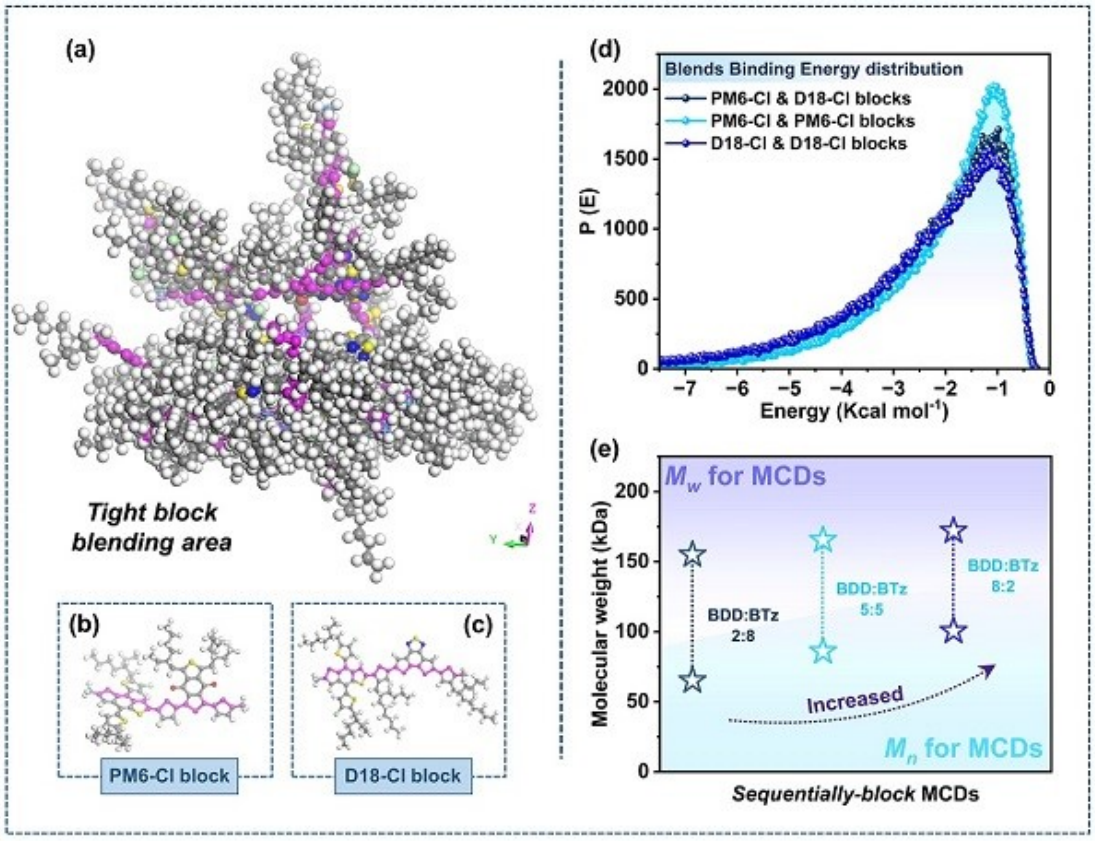

Figure S15. The blending binding energy result of electronic active blocks PM6-Cl (b) and D18-Cl (c) blocks: Simulation diagram of lowest energy blending with 50 pairs of PM6-Cl and D18-Cl blocks (a) and corresponding blends binding energy distribution between PM6-Cl and PM6-Cl blocks, PM6-Cl and D18-Cl blocks, and D18-Cl and D18-Cl blocks (d), both results were calculated based on **Materials Studio 8.0** at **Blends caculations**. The correlation between molecular weight and blending ratio in *sequentially-block* MCDs.

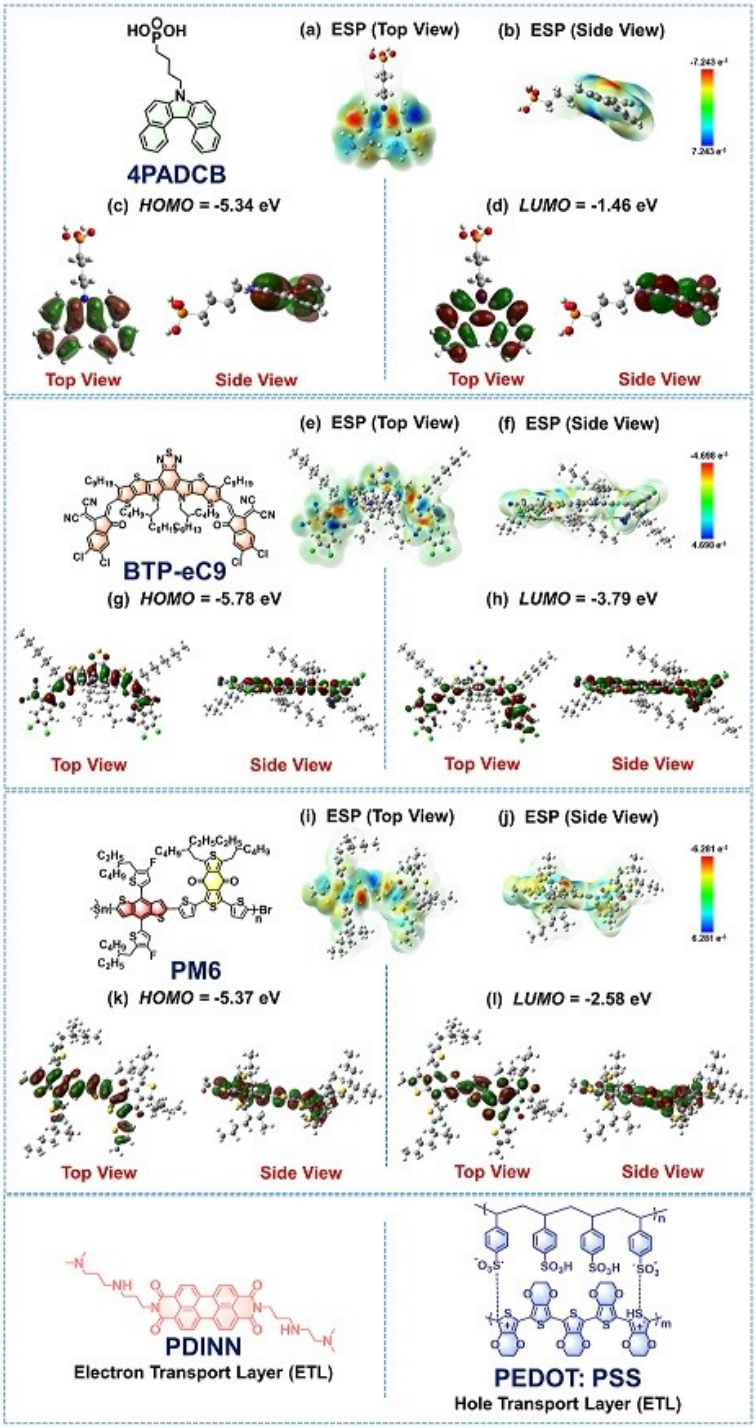

Figure S16. The detailed molecular structure of self-assembled molecule (SAM) **4PADCB**, acceptor **BTP-eC9**, donor **PM6**, electron transport layer **PDINN**, and hole transport layer **PEDOT: PSS** as well as theoretical calculations based on DFT theory at **B3LYP/6-31G (d, p) level**: ESP distribution in top view (a, e, and i) and side view (b, f, and j); *HOMO* (c, g, and k) and *LUMO* (d, h, and l) energy levels in top view and side view.

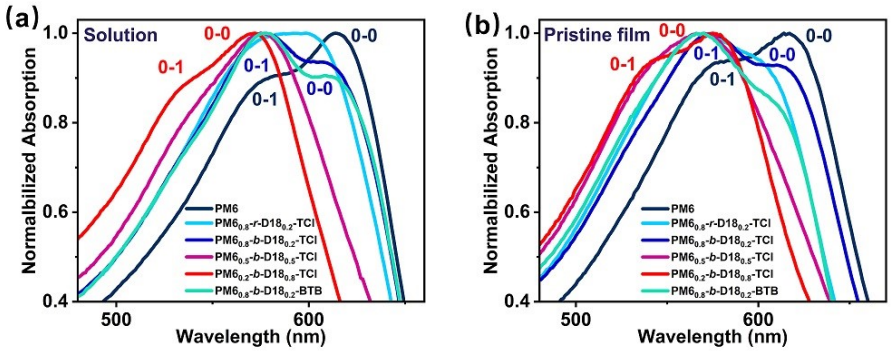

Figure S17. UV-vis-NIR absorption curve of partial enlarged image for MCDs **PM6**, **PM6-Cl$_{0.8}$-*r*-D18-Cl$_{0.2}$-TCl**, **PM6-Cl$_{0.8}$-*b*-D18-Cl$_{0.2}$-TCl**, **PM6-Cl$_{0.5}$-*b*-D18-Cl$_{0.5}$-TCl**, **PM6-Cl$_{0.2}$-*b*-D18-Cl$_{0.8}$-TCl**, and **PM6-Cl$_{0.8}$-*b*-D18-Cl$_{0.2}$-BTB** in solution (a) and film (b).

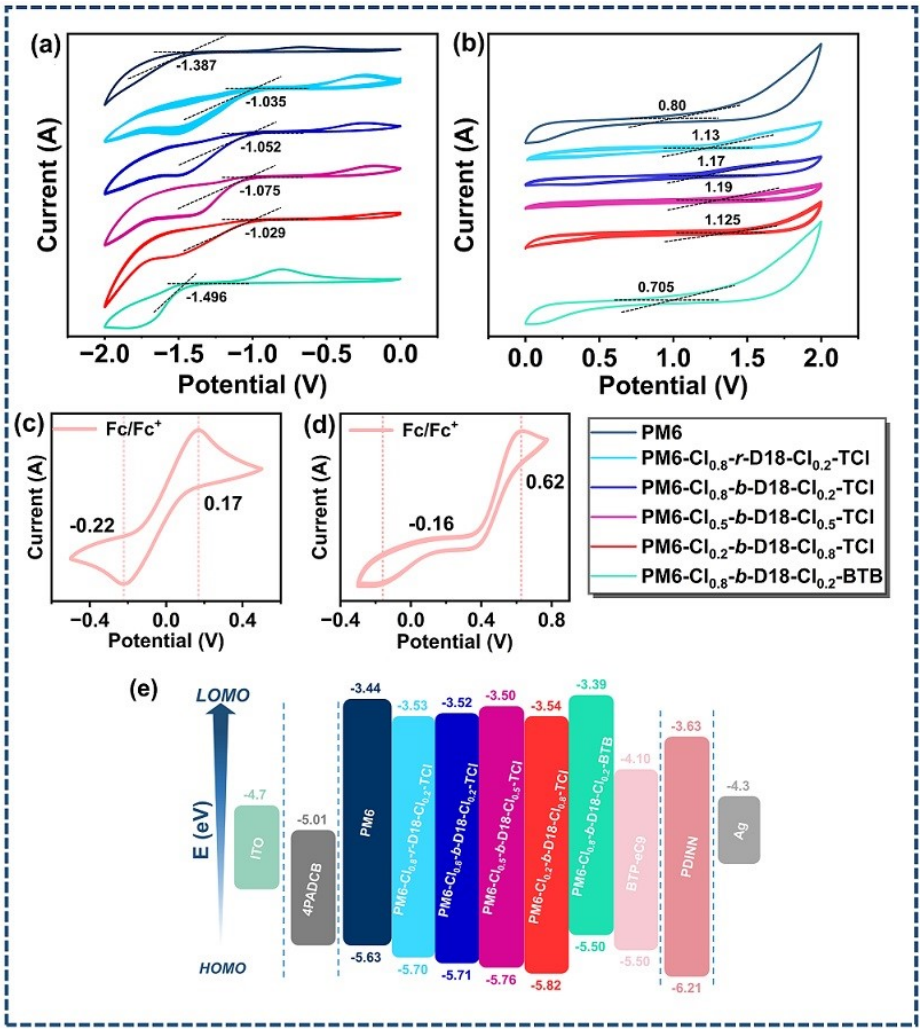

Figure S18. Cyclic voltammetry curves of **PM6**, **PM6-Cl$_{0.8}$-*r*-D18-Cl$_{0.2}$-TCl**, **PM6-Cl$_{0.8}$-*b*-D18-Cl$_{0.2}$-TCl**, **PM6-Cl$_{0.5}$-*r*-D18-Cl$_{0.5}$-TCl**, **PM6-Cl$_{0.2}$-*r*-D18-Cl$_{0.8}$-TCl**, and

PM6-$Cl_{0.8}$-*b*-D18-$Cl_{0.2}$-BTB (a, b); Fc/Fc^+ curve related on **PM6** and **$P1_{0.8}$-*b*-$P2_{0.2}$-BTB** (c); Fc/Fc^+ curve related on **$P1_{0.8}$-*r*-$P2_{0.2}$-TCl**, **$P1_{0.8}$-*b*-$P2_{0.2}$-TCl**, **$P1_{0.5}$-*b*-$P2_{0.5}$-TCl**, and **$P1_{0.2}$-*b*-$P2_{0.8}$-TCl** (d); The detailed *HOMO*/*LUMO* energy level values for corresponding MCD materials (e).

* By making tangent lines to the starting part of the oxidation current curve scanned in the positive potential direction and the starting part of the reduction current curve scanned in the negative potential direction on the cyclic voltammetry curve, the starting oxidation potential (φ_{ox}) and starting reduction potential (φ_{red}) values of MCDs can be obtained by intersecting the tangent lines with the horizontal axis. Therefore, the φ_{ox} values of **PM6**, **PM6-$Cl_{0.8}$-*r*-D18-$Cl_{0.2}$-TCl**, **PM6-$Cl_{0.8}$-*b*-D18-$Cl_{0.2}$-TCl**, **PM6-$Cl_{0.5}$-*r*-D18-$Cl_{0.5}$-TCl**, **PM6-$Cl_{0.2}$-*r*-D18-$Cl_{0.8}$-TCl**, and **PM6-$Cl_{0.8}$-*b*-D18-$Cl_{0.2}$-BTB** were -1.387 V, -1.035 V, -1.052 V, -1.075 V, -1.029 V, and -1.496 V in turn. The φ_{red} values of **PM6**, **PM6-$Cl_{0.8}$-*r*-D18-$Cl_{0.2}$-TCl**, **PM6-$Cl_{0.8}$-*b*-D18-$Cl_{0.2}$-TCl**, **PM6-$Cl_{0.5}$-*r*-D18-$Cl_{0.5}$-TCl**, **PM6-$Cl_{0.2}$-*r*-D18-$Cl_{0.8}$-TCl**, and **PM6-$Cl_{0.8}$-*b*-D18-$Cl_{0.2}$-BTB** were 0.80 V, 1.13 V, 1.17 V, 1.19 V, 1.125 V, and 0.705 V, respectively.

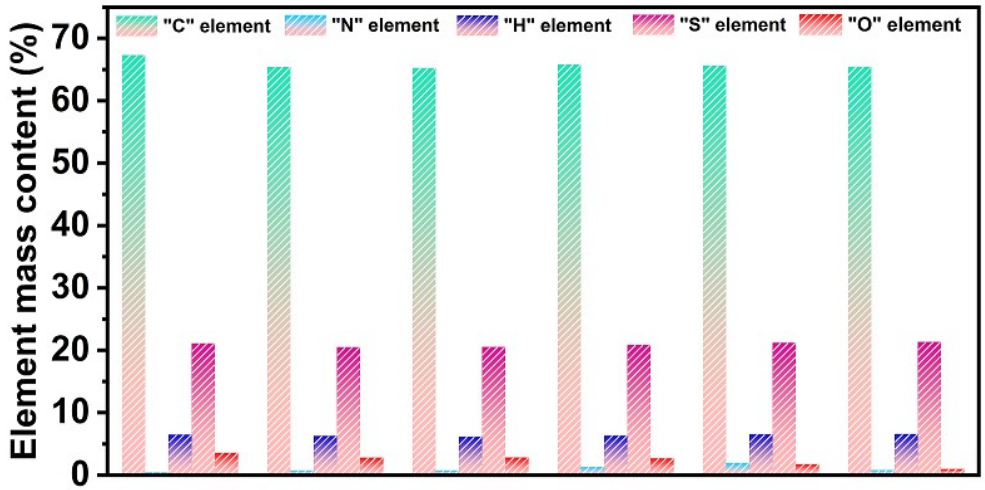

Figure S19. The elemental analysis characterization for **PM6**, **PM6-$Cl_{0.8}$-*r*-D18-$Cl_{0.2}$-TCl**, **PM6-$Cl_{0.8}$-*b*-D18-$Cl_{0.2}$-TCl**, **PM6-$Cl_{0.5}$-*b*-D18-$Cl_{0.5}$-TCl**, **PM6-$Cl_{0.2}$-*b*-D18-$Cl_{0.8}$-TCl**, and **PM6-$Cl_{0.8}$-*b*-D18-$Cl_{0.2}$-BTB**.

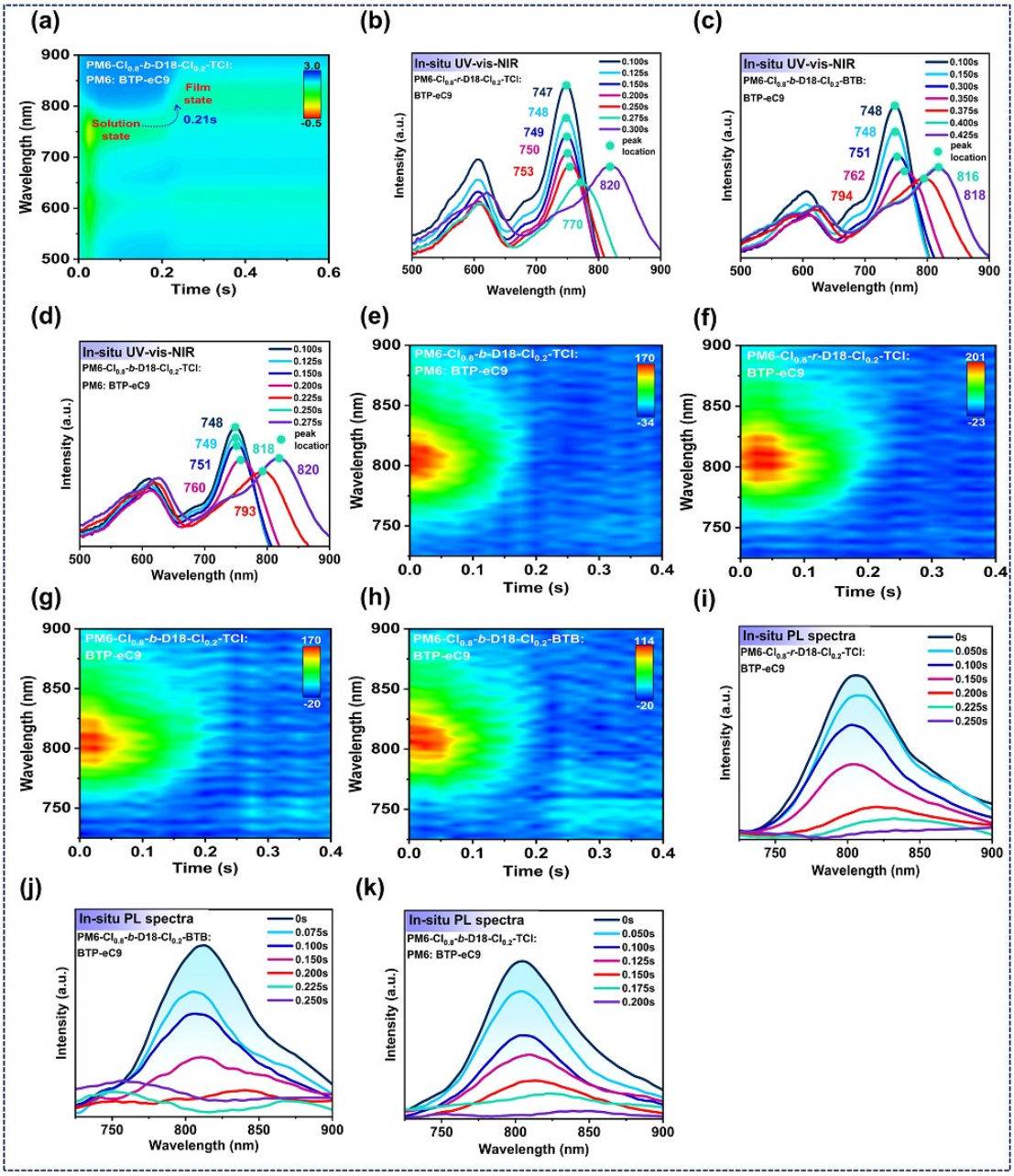

Figure S20. The 2D *in-situ* absorption spectra for **PM6-$Cl_{0.8}$-*b*-D18-$Cl_{0.2}$-TCl**: PM6-based blend system (a) as well as 1D *in-situ* absorption spectra characterization results for **PM6-$Cl_{0.8}$-*r*-D18-$Cl_{0.2}$-TCl**-based (b), **PM6-$Cl_{0.8}$-*b*-D18-$Cl_{0.2}$-BTB** (c), and **PM6-$Cl_{0.8}$-*b*-D18-$Cl_{0.2}$-TCl**: PM6-based (d) systems; 2D photoluminescence (PL) spectra characterization for **PM6-$Cl_{0.8}$-*r*-D18-$Cl_{0.2}$-TCl**-based (f), **PM6-$Cl_{0.8}$-*b*-D18-$Cl_{0.2}$-TCl**-based (g), **PM6-$Cl_{0.8}$-*b*-D18-$Cl_{0.2}$-BTB** (h), and **PM6-$Cl_{0.8}$-*b*-D18-$Cl_{0.2}$-TCl**: PM6-based (e) systems as well as corresponding 1D PL spectra characterization results (i-k).

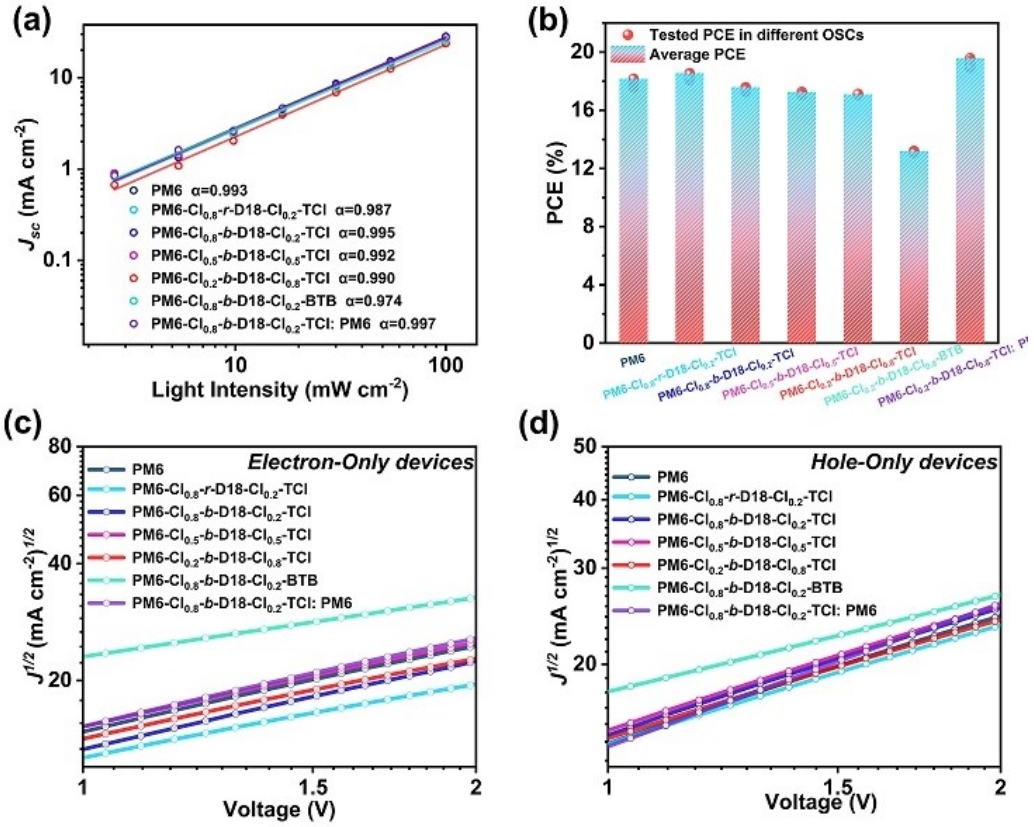

Figure S21. Light intensity dependence of J_{sc} for MCDs (a); The average PCE tested based on different MCD-based OSCs; SCLC test for hole (i) and electron (j) based on MCD-based OSCs.

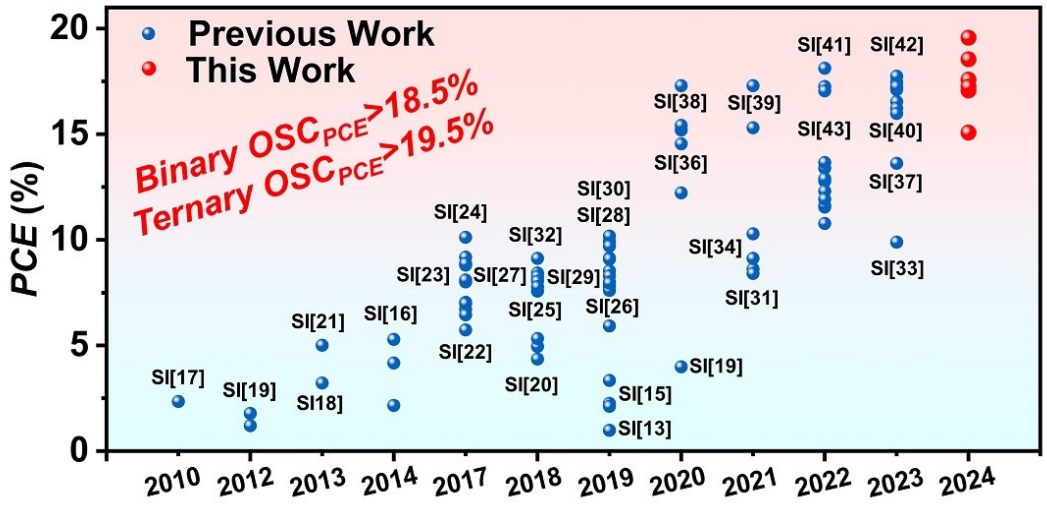

Figure 22. Evolution diagram of photovoltaic performance of MCD-based OSC, data sourced from **Table S2**.

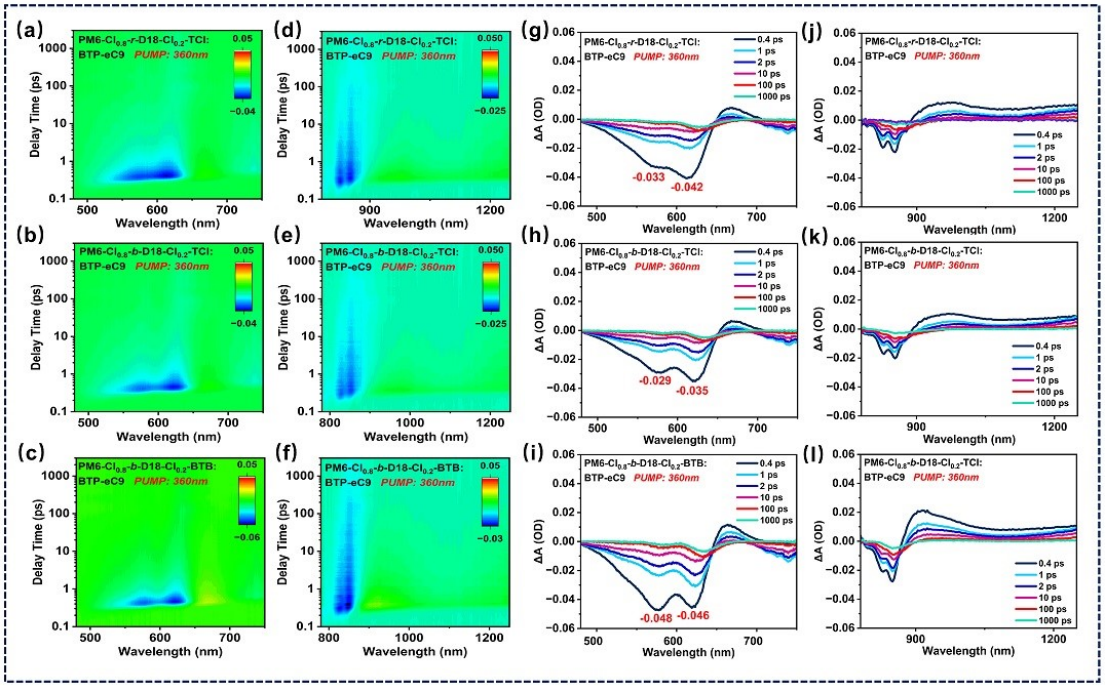

Figure S23. 2D TA image of the MCD: BTP-eC9 blend films for *random* MCD **PM6-$Cl_{0.8}$-*r*-D18-$Cl_{0.2}$-TCl** (a and d), *sequentially-block* MCD **PM6-$Cl_{0.8}$-*b*-D18-$Cl_{0.2}$-TCl** (b and e), and *flexible spacer-block* MCD **PM6-$Cl_{0.8}$-*b*-D18-$Cl_{0.2}$-BTB** (c and f) as well as 1D absorption spectrum at indicated delay times during the UV-visible absorption range (g, h, and i) and near-infrared absorption range (j, k, and l).

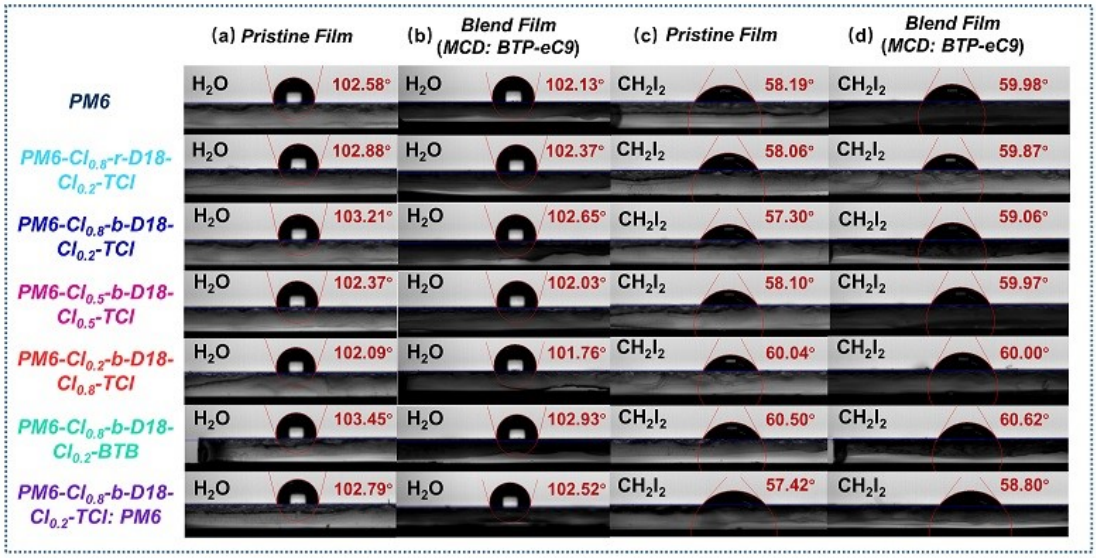

Figure S24. The contact angles of pristine MCD films in water (a) and diiodomethane (c) as well as MCD: BTP-eC9 blend films in in water (b) and diiodomethane (d).

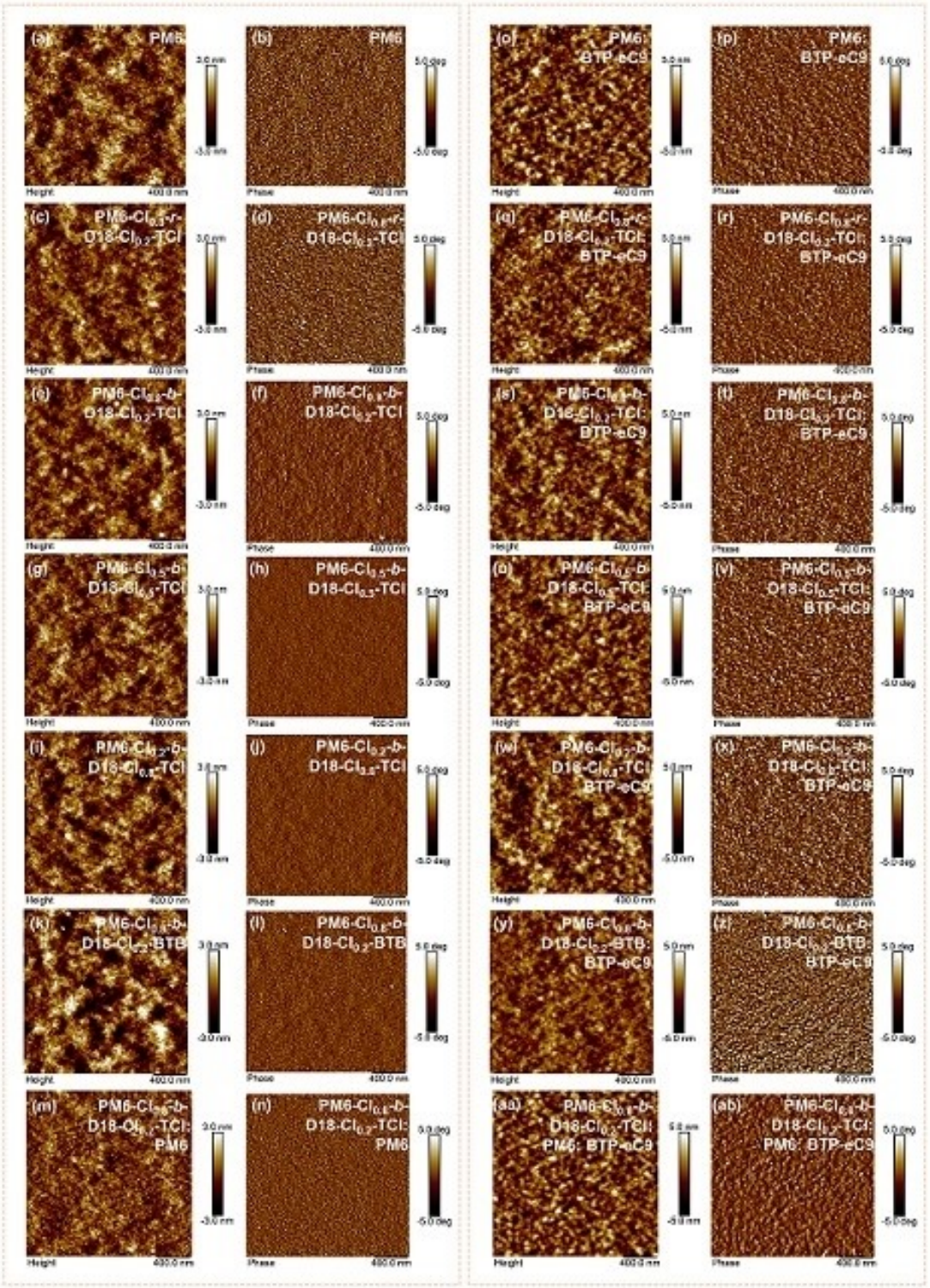

Figure S25. AFM characterization of hight figures (2 × 2 μm) and phase figures (2 × 2 μm) of pristine MCD films **PM6** (a, b), **PM6-Cl$_{0.8}$-*r*-D18-Cl$_{0.2}$-TCl** (c, d), **PM6-Cl$_{0.8}$-*b*-D18-Cl$_{0.2}$-TCl** (e, f), **PM6-Cl$_{0.5}$-*b*-D18-Cl$_{0.5}$-TCl** (g, h), **PM6-Cl$_{0.2}$-*b*-D18-Cl$_{0.8}$-TCl** (i, j), **PM6-Cl$_{0.8}$-*b*-D18-Cl$_{0.2}$-BTB** (k, l), and **PM6-Cl$_{0.8}$-*b*-D18-Cl$_{0.2}$-TCl: PM6** (m, n) as well as corresponding MCD: BTP-eC9 blend films **PM6: BTP-eC9** (o, p), **PM6-Cl$_{0.8}$-*r*-D18-Cl$_{0.2}$-TCl: BTP-eC9**

(q, r), **PM6-$Cl_{0.8}$-*b*-D18-$Cl_{0.2}$-TCl: BTP-eC9** (s, t), **PM6-$Cl_{0.5}$-*b*-D18-$Cl_{0.5}$-TCl: BTP-eC9: BTP-eC9: BTP-eC9** (u, v), **PM6-$Cl_{0.2}$-*b*-D18-$Cl_{0.8}$-TCl: BTP-eC9** (w, x), **PM6-$Cl_{0.8}$-*b*-D18-$Cl_{0.2}$-BTB: BTP-eC9** (y, z), and **PM6-$Cl_{0.8}$-*b*-D18-$Cl_{0.2}$-TCl: PM6: BTP-eC9** (aa, ab)**.**

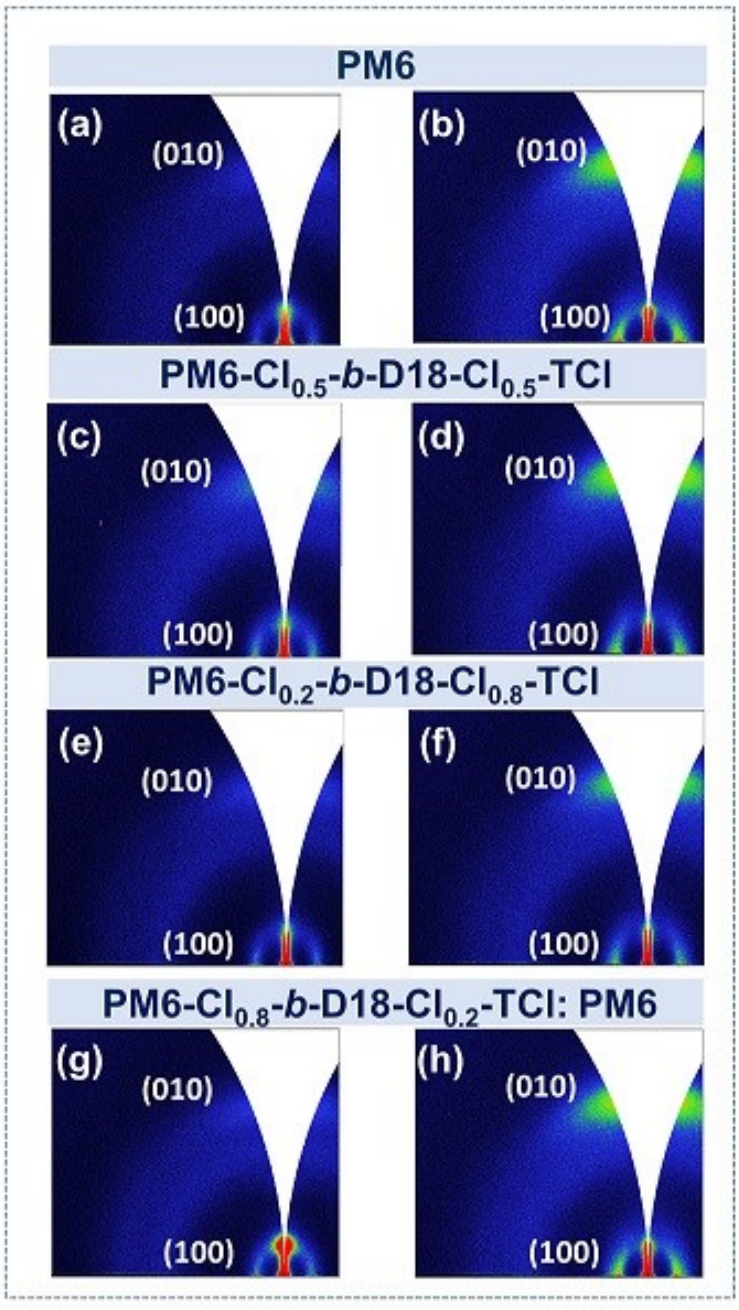

Figure S26. 2D GIWAXS characterization for **PM6**, **PM6-$Cl_{0.5}$-*b*-D18-$Cl_{0.5}$-TCl**, **PM6-$Cl_{0.2}$-*b*-D18-$Cl_{0.8}$-TCl**, and **PM6: PM6-$Cl_{0.8}$-*b*-D18-$Cl_{0.2}$-TCl** pristine films (a, c, e, and g) and corresponding blend films (b, d, f, and h).

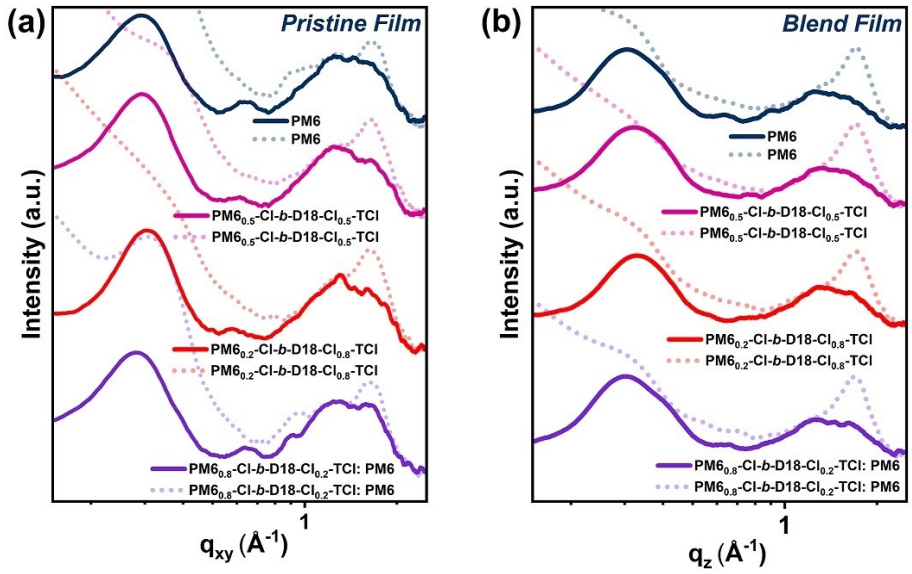

Figure S27. 1D GIWAXS characterization result of sequentially-block MCDs **PM6**, **PM6-Cl$_{0.5}$-*b*-D18-Cl$_{0.5}$-TCl**, **PM6-Cl$_{0.2}$-*b*-D18-Cl$_{0.8}$-TCl**, and **PM6: PM6-Cl$_{0.8}$-*b*-D18-Cl$_{0.2}$-TCl** in pristine (a) and blend (b) films.

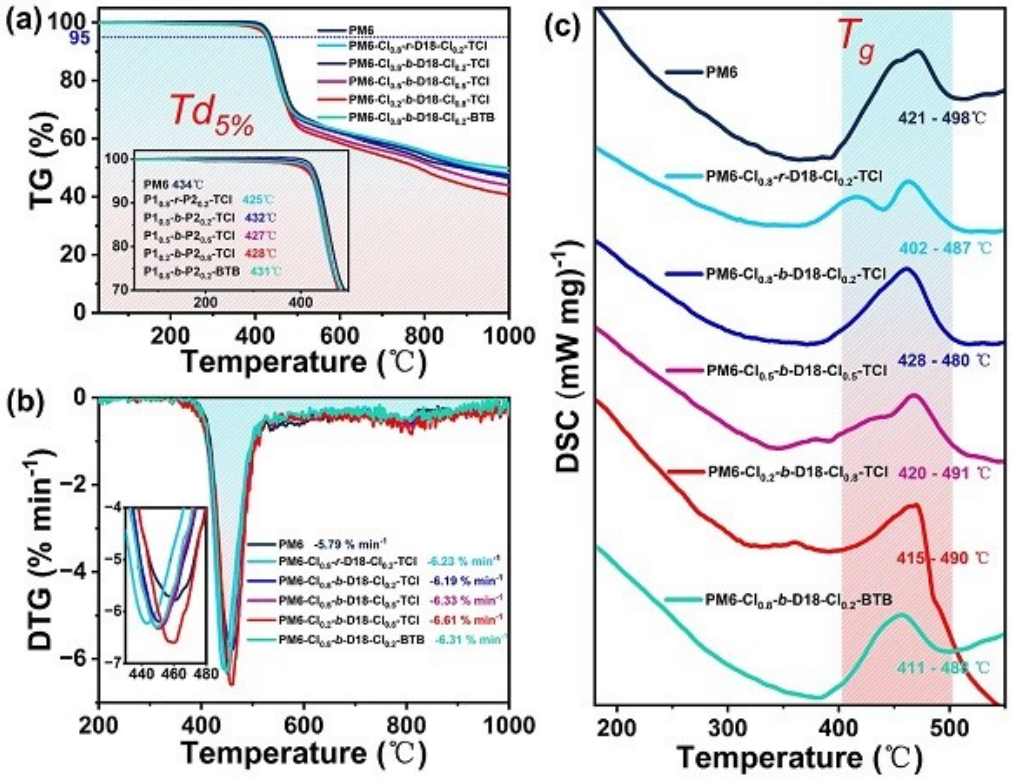

Figure S28. The thermo-gravimetric (TG) test for MCDs (a); the Derivative thermo-gravimetric (DTG) test for MCDs (b); the differential Scanning Calorimetry (DSC) test for MCDs (c).

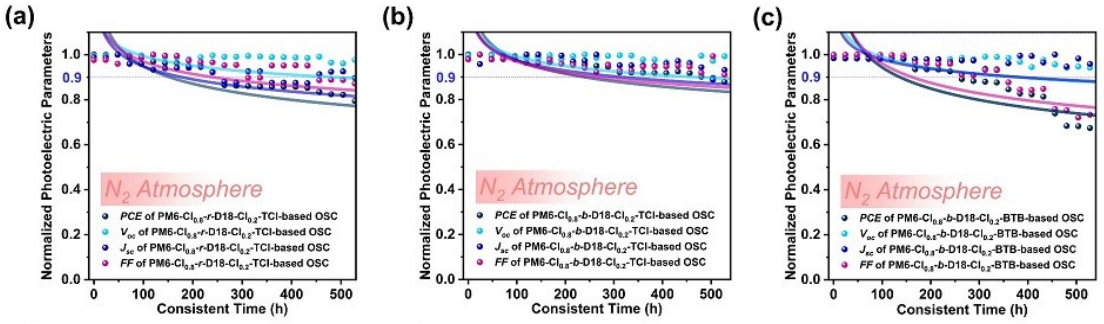

Figure S29. The detailed photoelectric stability of MCDs: BTP-eC9-based OSCs (a-c).

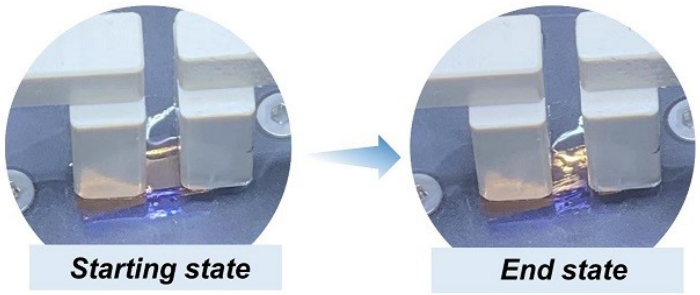

Figure S30. The pseudo free-standing tensile test in water.

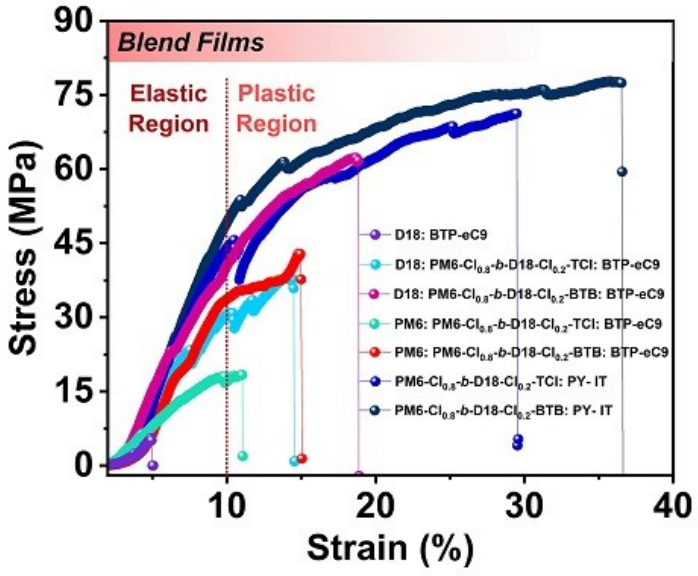

Figure S31. The pseudo-free-standing tensile test for blend films of D18: BTP-eC9, D18: **PM6-$Cl_{0.8}$-*b*-D18-$Cl_{0.2}$-TCl**, D18: **PM6-$Cl_{0.2}$-*b*-D18-$Cl_{0.8}$-BTB**, PM6: **PM6-$Cl_{0.8}$-*b*-D18-$Cl_{0.2}$-TCl**: BTP-eC9, PM6: **PM6-$Cl_{0.8}$-*b*-D18-$Cl_{0.2}$-BTB**: BTP-eC9, **PM6-$Cl_{0.8}$-*b*-D18-$Cl_{0.2}$-TCl**: PY-IT, and **PM6-$Cl_{0.8}$-*b*-D18-$Cl_{0.2}$-BTB**: PY-IT.

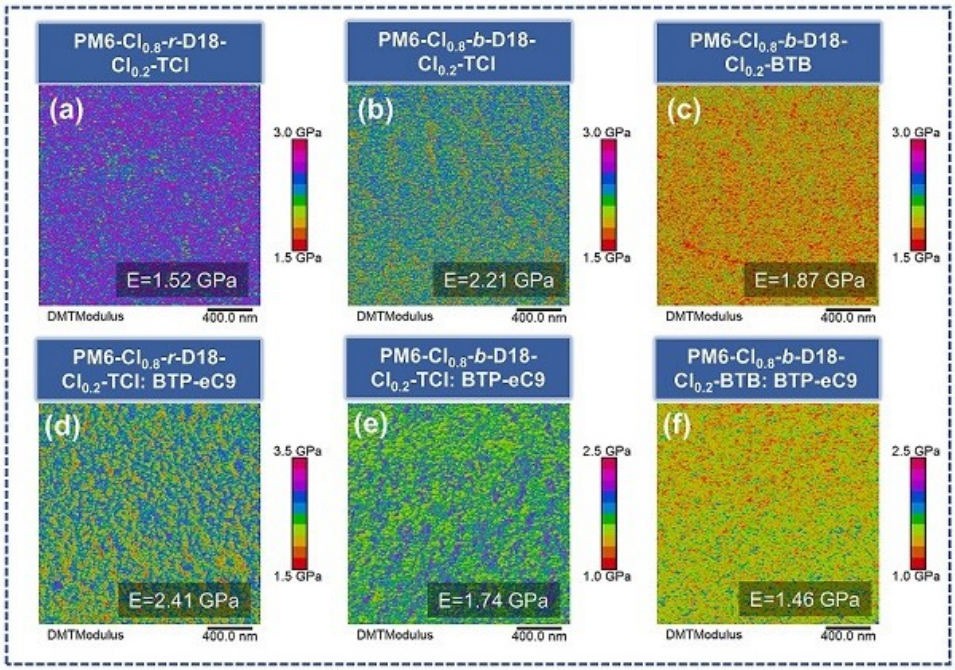

Figure S32. DMT modulus and adhesion of **PM6-C1$_{0.8}$-*r*-D18-Cl$_{0.2}$-TCl**, **PM6-C1$_{0.8}$-*b*-D18-Cl$_{0.2}$-TCl**, and **PM6-C1$_{0.8}$-*b*-D18-Cl$_{0.2}$-BTB** pristine (a, b, and c) and blend (d, e, and f) films obtain by the PFQNM method, with the scanned area is 2 μm × 2 μm.

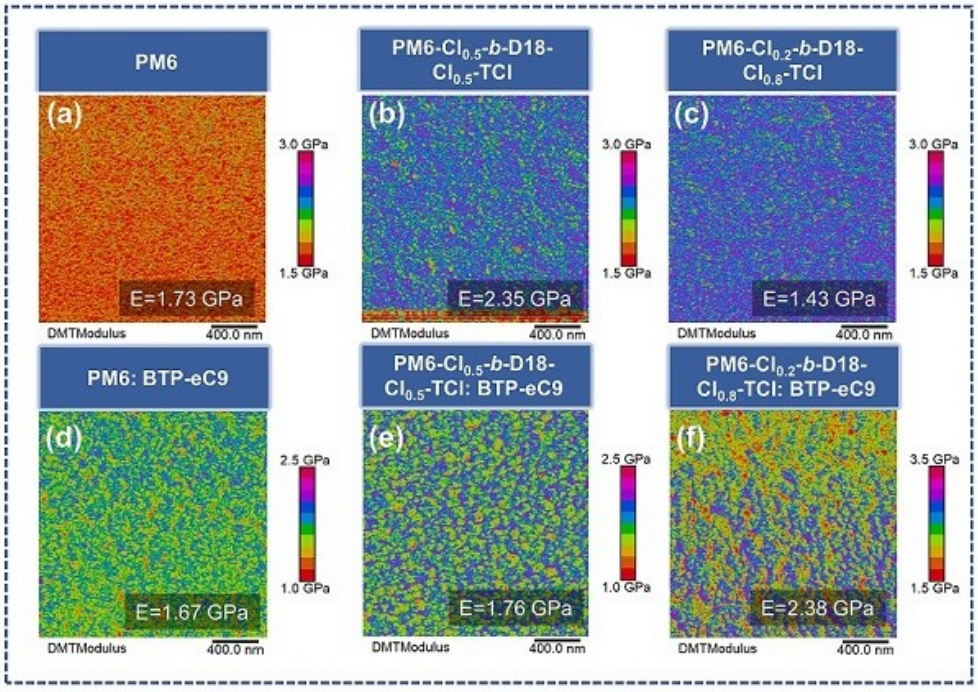

Figure S33. DMT modulus and adhesion of **PM6**, **PM6-C1$_{0.5}$-*b*-D18-Cl$_{0.5}$-TCl**, and **PM6-C1$_{0.2}$-*b*-D18-Cl$_{0.8}$-TCl** pristine (a, b, and c) and blend (d, e, and f) films obtain by the PFQNM

method, with the scanned area is 2 μm × 2 μm.

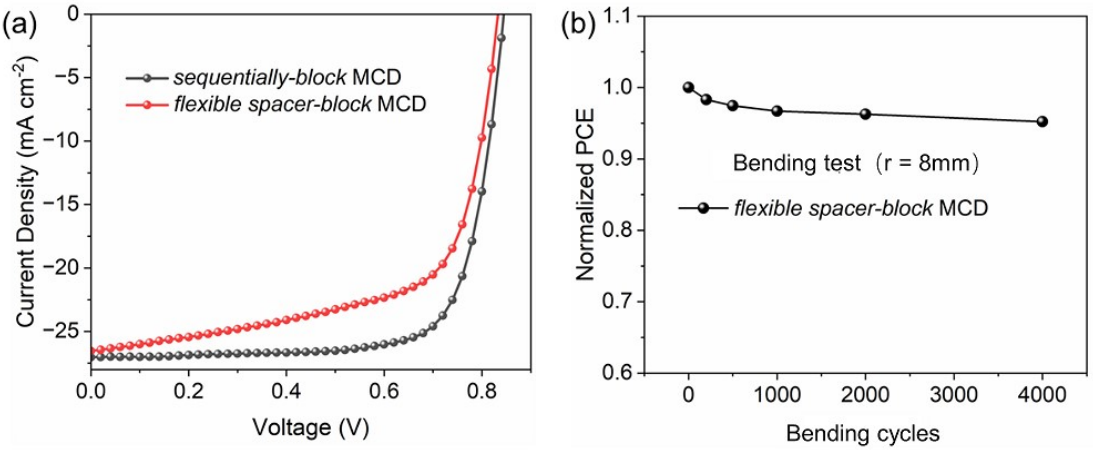

Figure S34. (a) J-V characterization of **PM6-Cl$_{0.8}$-*b*-D18-Cl$_{0.2}$-TCl**:BTP-eC9-based and **PM6-Cl$_{0.8}$-*b*-D18-Cl$_{0.2}$-BTB**:BTP-eC9-based flexible OSCs. (b) Decays of normalized PCEs of flexible devices in a continuous bending test with the blending radius of 8 mm.

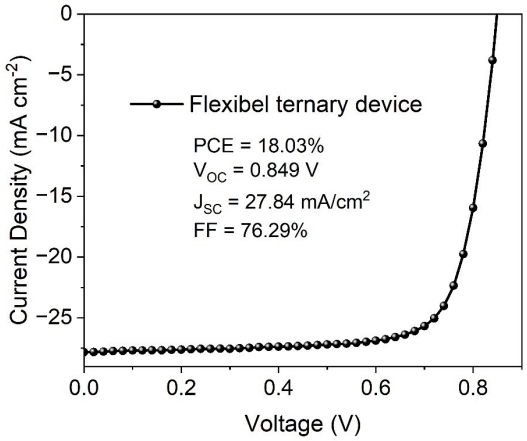

Figure S35. *J-V* characterization of **PM6-Cl$_{0.8}$-*b*-D18-Cl$_{0.2}$-TCl**: PM6: BTP-eC9-based flexible ternary OSCs.

Batch Name: 20240914
Acquired: 2024/9/14 9:26:51

Workbook Details
Eluent: TCB stabilised with 0.0125% BHT
Column Set: PLgel MIXED-B LS 300x7.5mm x2
Detector: RI
Flow Rate: 1.00 ml/min
Temperature: 150
Injection Volume: 200.0 ul

Analysis Using Method: 20240901
Comments:

Calibration Used: 2024/9/7 10:39:10
High Limit MW RT: 10.95 mins
High Limit MW: 6217712
K: 17.5000
Low Limit MW RT: 17.27 mins
Low Limit MW: 623
Alpha: 0.6700

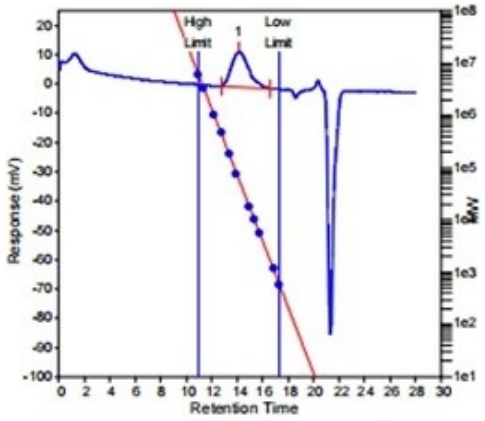

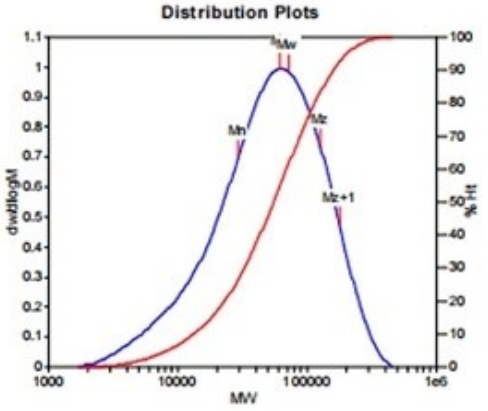

MW Averages

Peak No	Mp	Mn	Mw	Mz	Mz+1	Mv	PD
1	61520	29159	72418	126206	177686	64659	2.48356

Processed Peaks

Peak No	Name	Start RT (mins)	Max RT (mins)	End RT (mins)	Pk Height (mV)	% Height	Area (mV.secs)	% Area
1		12.75	14.10	16.58	12.0374	0	1145.06	100

Cirrus GPC Version 3.4 Page 1 2024/9/14 15:45

Figure S36. GPC characterization report of **PM6**.

Batch Name: 20240914
Acquired: 2024/9/14 12:02:25

Workbook Details
Eluent: TCB stabilised with 0.0125% BHT
Column Set: PLgel MIXED-B LS 300x7.5mm x2
Detector: RI
Flow Rate: 1.00 ml/min
Temperature: 150
Injection Volume: 200.0 ul

Analysis Using Method: 20240901
Comments:

Calibration Used: 2024/9/7 10:39:10
High Limit MW RT: 10.95 mins
High Limit MW: 6217712
K: 17.5000
Low Limit MW RT: 17.27 mins
Low Limit MW: 623
Alpha: 0.6700

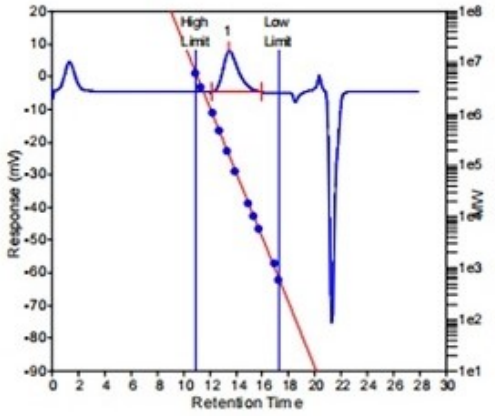

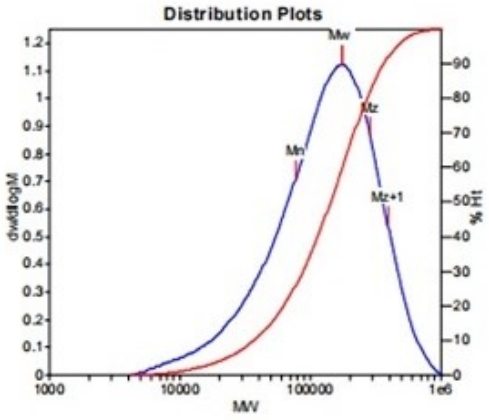

MW Averages

Peak No	Mp	Mn	Mw	Mz	Mz+1	Mv	PD
1	174860	76704	175347	284602	389976	158958	2.28602

Processed Peaks

Peak No	Name	Start RT (mins)	Max RT (mins)	End RT (mins)	Pk Height (mV)	% Height	Area (mV.secs)	% Area
1		12.18	13.40	15.95	12.6626	0	1068.23	100

Figure S37. GPC characterization report of **PM6-Cl$_{0.8}$-*r*-D18-Cl$_{0.2}$-TCl**.

Batch Name: 20240914
Acquired: 2024/9/14 10:29:05

Workbook Details
Eluent: TCB stabilised with 0.0125% BHT
Column Set: PLgel MIXED-B LS 300x7.5mm x2
Detector: RI
Flow Rate: 1.00 ml/min
Temperature: 150
Injection Volume: 200.0 ul

Analysis Using Method: 20240901
Comments:

Calibration Used: 2024/9/7 10:39:10
High Limit MW RT: 10.95 mins
High Limit MW: 6217712
K: 17.5000
Low Limit MW RT: 17.27 mins
Low Limit MW: 623
Alpha: 0.6700

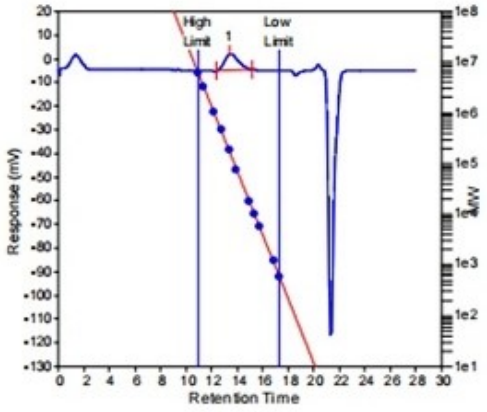

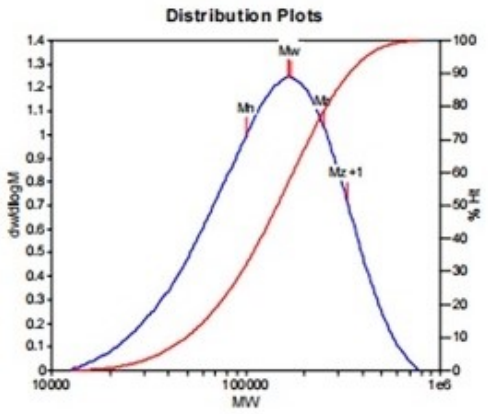

MW Averages

Peak No	Mp	Mn	Mw	Mz	Mz+1	Mv	PD
1	166567	100450	171869	253531	331107	159454	1.71099

Processed Peaks

Peak No	Name	Start RT (mins)	Max RT (mins)	End RT (mins)	Pk Height (mV)	% Height	Area (mV.secs)	% Area
1		12.38	13.43	15.20	7.09777	0	539.072	100

Cirrus GPC Version 3.4 Page 1 2024/9/14 15:45

Figure S38. GPC characterization report of **PM6-$Cl_{0.8}$-*b*-D18-$Cl_{0.2}$-TCl**.

Batch Name: 20240914
Acquired: 2024/9/14 9:57:58

Workbook Details
Eluent: TCB stabilised with 0.0125% BHT
Column Set: PLgel MIXED-B LS 300x7.5mm x2
Detector: RI
Flow Rate: 1.00 ml/min
Temperature: 150
Injection Volume: 200.0 ul

Analysis Using Method: 20240901
Comments:

Calibration Used: 2024/9/7 10:39:10
High Limit MW RT: 10.95 mins
High Limit MW: 6217712
K: 17.5000
Low Limit MW RT: 17.27 mins
Low Limit MW: 623
Alpha: 0.6700

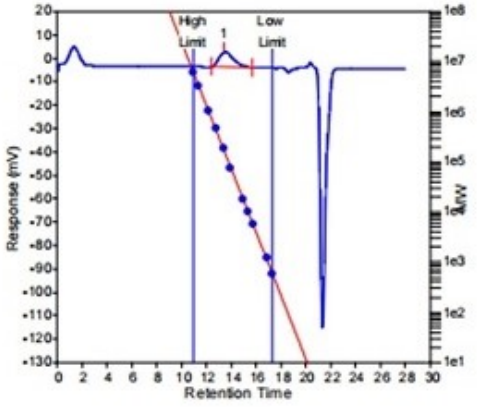

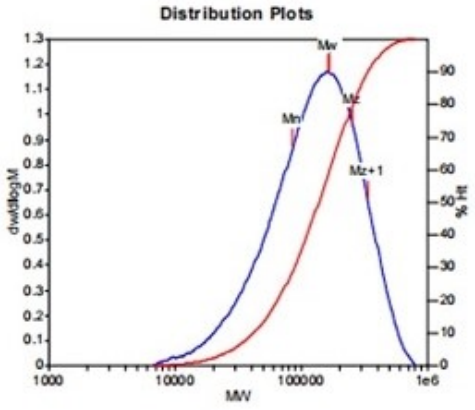

MW Averages

Peak No	Mp	Mn	Mw	Mz	Mz+1	Mv	PD
1	162570	85926	165393	253444	335050	151955	1.92483

Processed Peaks

Peak No	Name	Start RT (mins)	Max RT (mins)	End RT (mins)	Pk Height (mV)	% Height	Area (mV.secs)	% Area
1		12.37	13.45	15.63	6.58915	0	533.18	100

Cirrus GPC Version 3.4 Page 1 2024/9/14 15:45

Figure S39. GPC characterization report of **PM6-$Cl_{0.5}$-*b*-D18-$Cl_{0.5}$-TCl**.

Batch Name: 20240914
Acquired: 2024/9/14 11:00:12

Workbook Details
Eluent: TCB stabilised with 0.0125% BHT
Column Set: PLgel MIXED-B LS 300x7.5mm x2
Detector: RI
Flow Rate: 1.00 ml/min
Temperature: 150
Injection Volume: 200.0 ul

Analysis Using Method: 20240901
Comments:

Calibration Used: 2024/9/7 10:39:10
High Limit MW RT: 10.95 mins
High Limit MW: 6217712
K: 17.5000
Low Limit MW RT: 17.27 mins
Low Limit MW: 623
Alpha: 0.6700

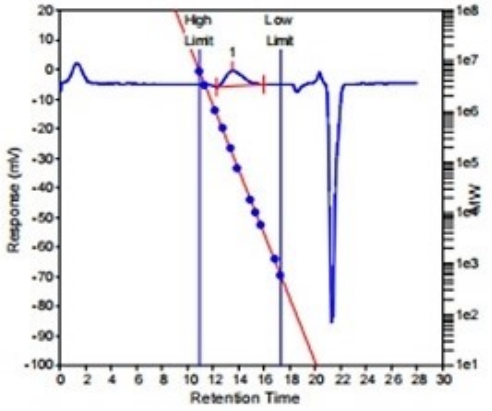

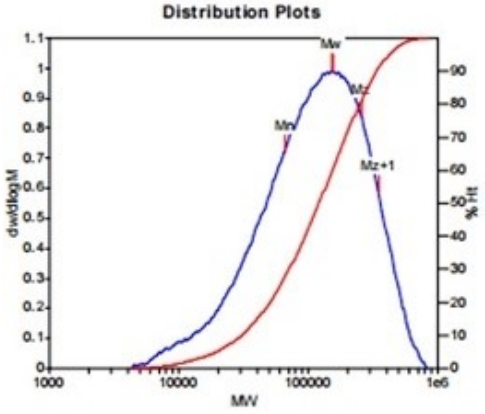

MW Averages

Peak No	Mp	Mn	Mw	Mz	Mz+1	Mv	PD
1	151143	65104	154959	258527	349705	139331	2.38018

Processed Peaks

Peak No	Name	Start RT (mins)	Max RT (mins)	End RT (mins)	Pk Height (mV)	% Height	Area (mV.secs)	% Area
1		12.33	13.50	15.93	5.05396	0	483.603	100

Cirrus GPC Version 3.4 Page 1 2024/9/14 15:45

Figure S40. GPC characterization report of **PM6-$Cl_{0.2}$-*b*-D18-$Cl_{0.8}$-TCl**.

Batch Name: 20240914
Acquired: 2024/9/14 12:33:31

Workbook Details
Eluent: TCB stabilised with 0.0125% BHT
Column Set: PLgel MIXED-B LS 300x7.5mm x2
Detector: RI
Flow Rate: 1.00 ml/min
Temperature: 150
Injection Volume: 200.0 ul

Analysis Using Method: 20240901
Comments:

Calibration Used: 2024/9/7 10:39:10
High Limit MW RT: 10.95 mins
High Limit MW: 6217712
K: 17.5000
Low Limit MW RT: 17.27 mins
Low Limit MW: 623
Alpha: 0.6700

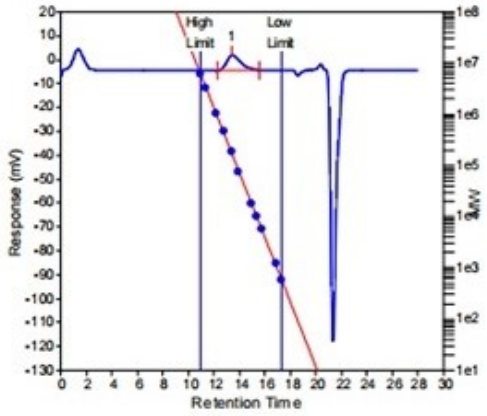

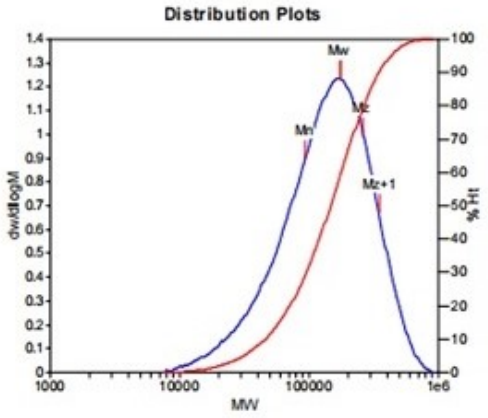

MW Averages

Peak No	Mp	Mn	Mw	Mz	Mz+1	Mv	PD
1	174860	93474	174045	262500	347523	160566	1.86196

Processed Peaks

Peak No	Name	Start RT (mins)	Max RT (mins)	End RT (mins)	Pk Height (mV)	% Height	Area (mV.secs)	% Area
1		12.27	13.40	15.57	6.4993	0	498.193	100

Cirrus GPC Version 3.4 Page 1 2024/9/14 15:46

Figure S41. GPC characterization report of **PM6-$Cl_{0.8}$-*b*-D18-$Cl_{0.2}$-BTB**.

Table S1. Detailed photoelectric and mechanical performance of reported MCD-based OSCs.

Active layer	Rigid OSC	Flexible OSC	Mechanical Performance	Ref.[b]
	PCE [%]	PCE [%]	COS[a] [%]	
PBQx-TF: MYT	15.71	11.80	10.3	[1]
PBQx-TF: DTBT-C0	17.01	12.74	17.3	[1]
PBDB-T: PYBDT	12.37	13.81	11.7	[2]
PBDB-T: PYT8T	9.70	12.18	3.9	[2]
PBDB-T: PYFS-Ran	11.83	8.17	18.1	[2]
PBDB-T: PYFS-Reg	15.84	10.64	22.4	[2]
PBDB-T: PYSiO-0	9.57	8.75	9.6	[3]
PBDB-T: PYSiO-5	11.28	(-)	13.9	[3]
PBDB-T: PYSiO-10	13.29	10.03	15.2	[3]
PBDB-T: PYSiO-20	11.75	(-)	17.6	[3]
PBDB-T: PYSiO-30	10.48	(-)	19.5	[3]
PBDB-T: PY-EH	10.25	8.2	11.15	[4]
PBDB-T: PY-SiO	11.48	9.8	18.32	[4]
D18: DYA-I	18.56	(-)	(-)	[5]
D18: DYA-IO	17.35	(-)	(-)	[5]
D18: DYA-O	16.27	(-)	(-)	[5]
PM6-*b*-$PDMS_{5k}$: L8-BO	17.02	11.80	4.30	[6]
PM6-*b*-$PDMS_{12k}$: L8-BO	17.93	11.19	8.13	[6]
PM6-*b*-$PDMS_{19k}$: L8-BO	17.53	11.17	18.14	[6]
PhAm3: Y7	16.52	(-)	10.4	[7]
PhAm5: Y7	17.28	12.21	13.8	[7]
PhAm10: Y7	15.80	(-)	22.6	[7]
PM6-OEG3: BTP-eC9	16.91	(-)	5.60	[8]
PM6-OEG5: BTP-eC9	17.34	11.78	10.50	[8]
PM6-OEG10: BTP-eC9	15.87	(-)	12.05	[8]
PM6-OEG20: BTP-eC9	12.31	(-)	7.66	[8]
D18: MYT	16.30	11.97	1.3	[9]
D18: DYT	17.14	(-)	(-)	[9]
D18: TYT-L	17.33	12.83	6.4	[9]
D18: TYT-S	18.48	14.37	21.6	[9]
$D18_{0.8}$-*r*-$PEHDT_{0.2}$: L8-BO	15.08	10.62	10.4	[10]

$D18_{0.8}$-*s*-$PEHDT_{0.2}$: L8-BO	18.73	14.02	17.2	[10]
PBDB-T: PYTS-0.0	12.82	12.82	(-)	[11]
PBDB-T: PYTS-0.1	14.04	14.04	(-)	[11]
PBDB-T: PYTS-0.3	14.35	14.35	(-)	[11]
PBDB-T: PYTS-0.5	7.68	7.68	(-)	[11]
PBDB-T: PYTS-1.0	1.64	1.64	(-)	[11]
$P1_{0.8}$/$P2_{0.2}$: Y6	16.95	15.66	8.01	[12]
$P1_{0.8}$/$P2_{0.2}$-TCl: Y6	18.15	17.03	9.09	[12]
$P1_{0.7}$/$P2_{0.3}$-TCl: Y6	17.40	(-)	9.15	[12]
$P1_{0.6}$/$P2_{0.4}$-TCl: Y6	17.18	(-)	12.3	[12]
PM6	**18.44**	**(-)**	**4.6**	**This work**
PM6-$Cl_{0.8}$-*r*-D18-$Cl_{0.2}$-TCl	**17.07**	**(-)**	**10.11**	**This work**
PM6-$Cl_{0.8}$-*b*-D18-$Cl_{0.2}$-TCl	**18.55**	**17.21**	**22.58**	**This work**
PM6-$Cl_{0.5}$-*b*-D18-$Cl_{0.5}$-TCl	**17.58**	**(-)**	**17.75**	**This work**
PM6-$Cl_{0.2}$-*b*-D18-$Cl_{0.8}$-TCl	**17.25**	**(-)**	**16.71**	**This work**
PM6-$Cl_{0.8}$-*b*-D18-$Cl_{0.2}$-BTB	**15.07**	**14.36**	**25.38**	**This work**
PM6-$Cl_{0.8}$-*b*-D18-$Cl_{0.2}$-TCl: PM6	**19.57**	**18.03**	**11.03**	**This work**

*(a) The facture strain value of blend films tested based on pseudo-free-standing tensile test on water.

Table S2. detailed photovoltaic performance in photovoltaic devices fabricated by MCDs.

MCD	Acceptor	V_{oc} [V]	J_{sc} [mA/cm]	*FF* [%]	PCE [%]	Ref.
PBDT-TPD-5	PNDI-T-5	0.79	2.7	46.1	0.98	[13]
PBDT-TPD-10	PNDO-T-5	0.8	5.5	51.3	2.26	[13]
PBDT-TPD-8	PNDI-T-5	0.81	7.6	54.3	3.34	[13]
PBDT-TPD-DPP20 %	$PC_{71}BM$	0.81	2.35	63	1.2	[14]
PBDT-TPD-DPP40 %	$PC_{71}BM$	0.67	5.02	53	1.78	[14]
PBDB-TBT4	ITIC	0.9	4.12	56.8	2.12	[15]
PBDB-TBT3	ITIC	0.91	11.45	56.91	5.93	[15]
PBDB-TBT2	ITIC	0.88	15.5	58.26	7.95	[15]
PBDB-TBT1	ITIC	0.86	16.84	62.85	9.09	[15]
P1	$PC_{61}BM$	0.72	6.16	49	2.16	[16]
P2	$PC_{61}BM$	0.74	12.21	46	4.17	[16]
P3	$PC_{61}BM$	0.78	14.13	48	5.29	[16]
P3	$PC_{70}BM$	0.71	6.41	51.7	2.35	[17]
P(BDT-TBTF/DPP)	$PC_{70}BM$	0.74	13.15	36	3.22	[18]
PBDTBD-25	IT-4F	0.83	11.96	42.16	3.99	[19]
PBDTBD-75	IT-4F	0.75	17.89	70.7	9.14	[19]
PBDTBD-50	IT-4F	0.8	17.16	73.1	9.7	[19]
P2FBT-50	$PC_{71}BM$	0.89	9.53	52	4.36	[20]
P2FBT-25	$PC_{71}BM$	0.89	10.52	54	4.95	[20]
P2FBT-75	$PC_{71}BM$	0.89	11.39	56	5.33	[20]
P4	$PC_{71}BM$	0.81	10.3	60	5.01	[21]
P6(0.1:0.9)	$PC_{71}BM$	0.71	13.65	61.1	5.74	[22]
P5(0.3:0.7)	$PC_{71}BM$	0.71	15.52	61.3	6.45	[22]
P2(0.9:0.1)	$PC_{71}BM$	0.74	14.7	64.4	6.72	[22]
P4(0.5:0.5)	$PC_{71}BM$	0.72	18.52	62.2	8.01	[22]
P3(0.7:0.3)	$PC_{71}BM$	0.73	18.45	66.9	8.8	[22]
LGC-D013	$PC_{71}BM$	0.87	11.29	73.13	6.99	[23]
[7-3]	$PC_{71}BM$	0.669	16.8	60.7	7.05	[24]
[1-1]	$PC_{71}BM$	0.664	18.4	65	8.1	[24]
[3-7]	$PC_{71}BM$	0.681	19.1	65.2	9.18	[24]
Ph75	ITIC	0.89	15.45	56.08	7.58	[25]
Ph25	ITIC	0.86	16.11	59.44	8.14	[25]
Ph50	ITIC	0.87	15.87	61.97	8.43	[25]
P2(2019)	$PC_{71}BM$	0.82	14.07	66	7.61	[26]
P4(2019)	$PC_{71}BM$	0.74	16.65	65	8	[26]
P3(2019)	$PC_{71}BM$	0.76	17.21	71	9.13	[26]
PBTTFB	$PC_{71}BM$	0.88	14.51	65	7.78	[27]
P12(2019)	$PC_{71}BM$	0.83	14.36	66	7.81	[28]
P14(2019)	$PC_{71}BM$	0.88	14.78	66	8.53	[28]
P13(2019)	$PC_{71}BM$	0.86	15.74	68	9.13	[28]
3MTT	ITIC	1	15.67	51.47	8.04	[29]
3MTB	ITIC	0.92	16.34	54.9	8.27	[29]

J52-TBF80	ITIC	0.756	16.76	66.6	8.3	[30]
J52-TBF20	ITIC	0.803	17.68	70.5	9.92	[30]
J52-TBF50	ITIC	0.79	17.93	72.8	10.18	[30]
P2(2020)	ITIC	0.925	15.9	57.2	8.41	[31]
P3(2020)	ITIC	0.913	16.87	59.2	9.12	[31]
P1(2020)	ITIC	0.946	15.94	57.2	8.62	[31]
D7A	ITIC	0.88	16.71	62	8.88	[32]
D3A	ITIC	0.87	16.58	65	9.12	[32]
D5A	ITIC	0.89	17.24	67	10.12	[32]
E18	BTA3-4F	1.3	10.95	68.66	9.89	[33]
P75	Y6	0.81	22.6	58	10.28	[34]
PCE10-BDT2Cl-0.3	Y6	0.7	23.56	66.24	10.77	[35]
PCE10-BDT2F-0.3	Y6	0.678	26.1	66.56	11.55	[35]
PCE10-BDT2Cl-0.5	Y6	0.724	23.37	64.41	11.62	[35]
PCE10-BDT2Cl-0.7	Y6	0.743	24.85	65.58	11.93	[35]
PCE10-BDT2F-0.6	Y6	0.739	26.01	64.08	12.3	[35]
PCE10-BDT2F-0.5	Y6	0.72	26.01	69.42	12.78	[35]
PCE10-BDT2F-0.9	Y6	0.766	25.14	67.71	12.89	[35]
PCE10-BDT2F-0.7	Y6	0.746	26.17	68.95	13.39	[35]
PCE10-BDT2F-0.8	Y6	0.753	26.36	69.45	13.66	[35]
PBDB-Th2Cl15	Y6	0.87	24.93	58.1	12.22	[36]
PBDB-Th15	Y6	0.83	24.8	72.33	14.54	[36]
PBDB-ThCl15	Y6	0.84	25.21	74.03	15.42	[36]
PBDB-T-2F(3/4)	Y6-HU	0.86	23.78	70	13.62	[37]
PM2(X:Y=1:1)	Y6	0.9	24.9	69	15.2	[38]
PM1(X:Y=4:1)	Y6	0.87	25.9	78	17.3	[38]
PM6-TZ40 (n: m = 60:40)	Y6	0.85	24.8	72	15.3	[39]
PM6-TZ20 (n: m = 80:20)	Y6	0.86	26.2	75	17.3	[39]
PM6-T-C12	Y6	0.843	25.97	73.02	15.98	[40]
PM6-T-C6	Y6	0.847	26.07	73.53	16.23	[40]
PM6-T-C1	Y6	0.847	25.89	75.44	16.54	[40]
PM6-T	Y6	0.85	26	77.4	17.11	[40]
D18-40%Cl	Y6	0.866	26.34	75.46	17.05	[41]
D18-20%Cl	Y6	0.861	27.2	78.06	18.12	[41]
PMD-5	L8-BO	0.892	25.16	76.61	17.19	[42]
PMD-20	L8-BO	0.907	25.53	76.14	17.26	[42]
PMD-10	L8-BO	0.895	25.44	76.72	17.47	[42]
PMD-15	L8-BO	0.899	25.64	77.01	17.75	[42]
PM6TPO	Y6	0.843	26.35	77.68	17.26	[43]
PM6	**BTP-eC9**	**0.846**	**28.22**	**77.19**	**18.44**	**This work**
PM6-$Cl_{0.8}$-*r*-D18-$Cl_{0.2}$-TCl	**BTP-eC9**	**0.853**	**27.4**	**73.04**	**17.07**	**This Work**
PM6-$Cl_{0.8}$-*b*-D18-$Cl_{0.2}$-TCl	**BTP-eC9**	**0.854**	**28.24**	**76.96**	**18.55**	**This Work**
PM6-$Cl_{0.5}$-*b*-D18-$Cl_{0.5}$-TCl	**BTP-eC9**	**0.860**	**27.54**	**74.22**	**17.58**	**This Work**
PM6-$Cl_{0.2}$-*b*-D18-$Cl_{0.8}$-TCl	**BTP-eC9**	**0.861**	**27.31**	**73.40**	**17.25**	**This work**
PM6-$Cl_{0.8}$-*b*-D18-$Cl_{0.2}$-BTB	**BTP-eC9**	**0.836**	**26.94**	**66.88**	**15.07**	**This Work**

PM6-$Cl_{0.8}$-*b*-D18-$Cl_{0.2}$-TCl: PM6	**BTP-eC9**	**0.864**	**28.86**	**78.40**	**19.57**	**This Work**

Table S3. Monomer reactivity for electronic active blocks **D18-Cl (BTz unit)** and **PM6-Cl (BDD unit)** in *sequentially-block* MCDs.

Ratio of BDD unit: BTz unit [%]	M_n **[kDa]**	M_w **[kDa]**
80: 20	100.4	171.9
50: 50	85.9	165.4
20: 80	65.1	154.9

Table S4. Detailed Photovoltaic parameters of MCDs and acceptor.

Materials	$\lambda_{max,s}$ [a] **[nm]**	$\lambda_{max,f}$ [b] **[nm]**	$\lambda_{onset,f}$ [c] **[nm]**	***HOMO*** [d] **[eV]**	***LUMO*** [d] **[eV]**	Eg^{cv} [e] **[eV]**
BTP-eC9	(-)	(-)	(-)	-5.78	-3.79	1.99
PM6	614	617	684	-5.63	-3.44	2.19
PM6-$Cl_{0.8}$-*r*-D18-$Cl_{0.2}$-TCl	570	571	688	-5.70	-3.53	2.17
PM6-$Cl_{0.8}$-*b*-D18-$Cl_{0.2}$-TCl	575	577	681	-5.71	-3.52	2.22
PM6-$Cl_{0.5}$-*b*-D18-$Cl_{0.5}$-TCl	573	574	677	-5.76	-3.50	2.26
PM6-$Cl_{0.2}$-*b*-D18-$Cl_{0.8}$-TCl	570	573	651	-5.82	-3.54	2.28
PM6-$Cl_{0.8}$-*b*-D18-$Cl_{0.2}$-BTB	572	572	683	-5.50	-3.39	2.11

*(a) the maximum absorption wavelength of donors in solution;

(b) the maximum absorption wavelength of donors in film;

(c) the onset absorption wavelength of donors in film;

(d) calculations based on DFT theory at **B3LYP/6-31G (d, p)** level;

(e) $Eg^{cv} = E_{HOMO} - E_{LUMO}$.

Table S5. Elemental analysis characterization result of "**C**", "**N**", "**H**", "**S**", and "**O**".

Blend film	Theoretical elemental content					Tested elemental content				
	C[(a)] [%]	N[(a)] [%]	H[(a)] [%]	S[(a)] [%]	O[(a)] [%]	C [%]	N [%]	H[(b)] [%]	S [%]	O[(b)] [%]
PM6	67.27	0	6.61	20.52	2.56	67.31	0.46	6.51	21.13	3.59
PM6-$Cl_{0.8}$-*r*-D18-$Cl_{0.2}$-TCl	65.30	0.44	6.27	20.48	1.99	65.38	0.72	6.28	20.50	2.8
PM6-$Cl_{0.8}$-*b*-D18-$Cl_{0.2}$-TCl	65.30	0.44	6.27	20.48	1.99	65.25	0.76	6.15	20.56	2.83
PM6-$Cl_{0.5}$-*b*-D18-$Cl_{0.5}$-TCl	65.40	1.06	6.43	20.55	1.21	65.81	1.32	6.34	20.88	2.69
PM6-$Cl_{0.2}$-*b*-D18-$Cl_{0.8}$-TCl	65.50	1.64	6.59	20.62	0.47	65.63	1.94	6.56	21.22	1.76
PM6-$Cl_{0.8}$-*b*-D18-$Cl_{0.2}$-BTB	64.70	1.00	6.37	21.73	1.14	65.44	0.81	6.60	21.36	0.99

*(a) calculated based on ideal copolymer molecular structure.

(b) The high content of hydrogen and oxygen elements is related to the moisture content in the air, so try to keep the sample dry as much as possible.

Table S6. Detailed photoelectric parameters for MCD-based OSCs with hole transport layer (HTL) **PEDOT: PSS 4083**.

MCD	Acceptor	D/A[(a)]	V_{oc} [V]	J_{sc} [mA cm^{-2}]	*FF* [%]	PCE [%]
PM6	BTP-eC9	1: 1.2	0.837	27.39	74.40	17.06
PM6-$Cl_{0.8}$-*r*-D18-$Cl_{0.2}$-TCl	BTP-eC9	1: 1.2	0.859	25.67	72.78	16.05
PM6-$Cl_{0.8}$-*b*-D18-$Cl_{0.2}$-TCl	BTP-eC9	1: 1.2	0.863	27.50	72.16	17.15
PM6-$Cl_{0.5}$-*b*-D18-$Cl_{0.5}$-TCl	BTP-eC9	1: 1.2	0.865	26.39	74.38	16.97
PM6-$Cl_{0.2}$-*b*-D18-$Cl_{0.8}$-TCl	BTP-eC9	1: 1.2	0.875	25.42	68.71	15.29
PM6-$Cl_{0.8}$-*b*-D18-$Cl_{0.2}$-BTB	BTP-eC9	1: 1.2	0.841	26.29	67.44	14.90
PM6-$Cl_{0.8}$-*b*-D18-$Cl_{0.2}$-TCl: PM6	BTP-eC9	0.1: 0.9: 1.2	0.865	27.53	72.21	17.20

*(a) The weight ratio of MCD to acceptor.

Table S7. Detailed photoelectric performance based on MCD-based OSCs.

MCD	P (E, T) [%]	α [%]	S [kT q^{-1}]	μ_h [cm^2 Vs^{-1}]	μ_e [cm^2 Vs^{-1}]	μ_h/μ_e [%]
PM6	0.993	99.3	1.19	3.28×10^{-3}	5.18×10^{-3}	63.3
PM6-$Cl_{0.8}$-*r*-D18-$Cl_{0.2}$-TCl	0.986	98.7	1.24	2.84×10^{-3}	4.74×10^{-3}	60.0
PM6-$Cl_{0.8}$-*b*-D18-$Cl_{0.2}$-TCl	0.994	99.5	1.19	3.15×10^{-3}	4.94×10^{-3}	63.8
PM6-$Cl_{0.5}$-*b*-D18-$Cl_{0.5}$-TCl	0.991	99.2	1.20	3.04×10^{-3}	4.86×10^{-3}	62.6
PM6-$Cl_{0.2}$-*b*-D18-$Cl_{0.8}$-TCl	0.990	99.0	1.23	2.87×10^{-3}	4.70×10^{-3}	61.1
PM6-$Cl_{0.8}$-*b*-D18-$Cl_{0.2}$-BTB	0.971	97.4	1.30	1.87×10^{-3}	3.20×10^{-3}	58.4
PM6-$Cl_{0.8}$-*b*-D18-$Cl_{0.2}$-TCl: PM6	0.997	99.7	1.15	3.62×10^{-3}	5.33×10^{-3}	67.9

Table S8. Detailed morphology parameters in MCD pristine and blend films.

Active Layer	θH_2O[a] [°]	θCH_2I_2[b] [°]	γ^d [mN m^{-1}]	γ^p [mN m^{-1}]	Surface tension [mN m^{-1}]	χ[c]	Ra[d] [nm]
PM6	102.80	58.19	30.052	0.162	30.214	1.282	0.790
PM6-$Cl_{0.8}$-*r*-D18-$Cl_{0.2}$-TCl	102.88	58.06	30.215	0.135	30.349	1.254	0.674
PM6-$Cl_{0.8}$-*b*-D18-$Cl_{0.2}$-TCl	103.21	57.30	30.822	0.092	30.913	1.143	0.685
PM6-$Cl_{0.5}$-*b*-D18-$Cl_{0.5}$-TCl	102.37	58.10	30.064	0.177	30.240	1.276	0.689
PM6-$Cl_{0.2}$-*b*-D18-$Cl_{0.8}$-TCl	102.09	60.04	28.658	0.280	28.939	1.561	0.768
PM6-$Cl_{0.8}$-*b*-D18-$Cl_{0.2}$-BTB	103.45	60.50	28.662	0.169	28.831	1.586	1.18
$P1_{0.8}$-*b*-$P2_{0.2}$-TCl: PM6	102.79	57.42	30.636	0.122	30.758	1.173	0.616
PM6: BTP-eC9	102.13	59.98	28.709	0.273	28.982	(-)	1.26
PM6-$Cl_{0.8}$-*r*-D18-$Cl_{0.2}$-TCl: BTP-eC9	102.37	59.87	28.842	0.244	29.086	(-)	1.11
PM6-$Cl_{0.8}$-*b*-D18-$Cl_{0.2}$-TCl: BTP-eC9	102.65	59.06	29.467	0.186	29.654	(-)	1.16
PM6-$Cl_{0.5}$-*b*-D18-$Cl_{0.5}$-TCl: BTP-eC9	102.03	59.97	28.692	0.284	28.976	(-)	1.10
PM6-$Cl_{0.2}$-*b*-D18-$Cl_{0.8}$-TCl: BTP-eC9	101.76	60.00	28.608	0.315	28.923	(-)	1.25
PM6-$Cl_{0.8}$-*b*-D18-$Cl_{0.2}$-BTB: BTP-eC9	102.93	60.62	28.456	0.220	28.676	(-)	1.30
PM6-$Cl_{0.8}$-*b*-D18-$Cl_{0.2}$-TCl: PM6: BTP-eC9	102.53	58.80	29.616	0.188	29.804	(-)	1.18
BTP-eC9[44]	96.9	34.3	43.919	0.023	43.942	(-)	(-)

*(a) The contact angle between H_2O and corresponding film;

(b) The contact angel between CH_2I_2 and corresponding films;

(c) $\chi=(\sqrt{\gamma_A}-\sqrt{\gamma_D})^2$, γ_A and γ_D represent the surface tension of the acceptor and donor, respectively.

The contact angle test obtains the compatibility of the material to the receptor, and the contact angle of the material is measured using water and ethylene glycol as non-polar solvents. The surface tension of different components is calculated by the following formula:

H_2O: London dispersion (γ^d) = 21.80 mN m^{-1}, polar (γ^p) = 51.0 mN m^{-1}.

CH_2I_2: London dispersion (γ^d) = 48.50 mN m^{-1}, polar (γ^p) = 2.30 mN m^{-1}.

(d) The value of **Ra** is calculated based on the characterization of AFM height figures in **Figure S22**, using the analysis software **Nano Scope Analysis 1.5**.

Table S9. Detailed GIWAXS characterization results of MCDs.

Active layer	**π-π stacking (Out-Of-Plane (OOP))**				**Lamellar stacking (In-Plane (IP))**			
	q_z[(a)] [Å]	d_π[(b)] [Å]	*FWHM*[(c)] [Å^{-1}]	*CCL*[(d)] [Å]	q_{xy}[(e)] [Å]	$d_{lamellar}$[(f)] [Å]	*FWHM* [Å^{-1}]	*CCL* [Å]
PM6	1.64	3.831	0.289	19.567	0.297	21.156	0.0869	65.073
PM6-Cl$_{0.5}$-*b*-D18-Cl$_{0.5}$-TCl	1.66	3.785	0.297	19.040	0.294	21.371	0.0852	66.372
PM6-Cl$_{0.2}$-*b*-D18-Cl$_{0.8}$-TCl	1.67	3.762	0.318	17.783	0.304	20.668	0.0946	59.777
PM6-Cl$_{0.8}$-*b*-D18-Cl$_{0.2}$-TCl: PM6	1.65	3.808	0.270	20.944	0.279	22.520	0.0802	70.510
PM6: BTP-eC9	1.70	3.696	0.279	20.268	0.303	20.737	0.0777	72.778
PM6-Cl$_{0.5}$-*b*-D18-Cl$_{0.5}$-TCl: BTP-eC9	1.72	3.653	0.285	19.842	0.320	19.635	0.0815	69.385
PM6-Cl$_{0.2}$-*b*-D18-Cl$_{0.8}$-TCl: BTP-eC9	1.73	3.632	0.289	19.567	0.330	19.040	0.0888	63.681
PM6-Cl$_{0.8}$-*b*-D18-Cl$_{0.2}$-TCl: PM6: BTP-eC9	1.71	3.674	0.260	21.749	0.296	21.227	0.0754	74.998

*(a) (010) π-π stacking diffraction peaks from the line cuts in the OOP direction;

(b) π-π stacking distance;

(c) Full width at half maxima;

(d) Conjugated crystal length;

(e) (100) Lamellar stacking diffraction peaks from the line cuts in the IP direction;

(f) Lamellar stacking distance.

Table S10. Detailed stability parameters of MCDs.

MCD	$Td_{5\%}$ [a] [°C]	$T_{DTG,\,m}$ [b] [°C]	DTG_m [c] [% min^{-1}]	T_g [d] [°C]
PM6	434	461	-5.79	421-498
PM6-$Cl_{0.8}$-*r*-D18-$Cl_{0.2}$-TCl	425	444	-6.23	402-487
PM6-$Cl_{0.8}$-*b*-D18-$Cl_{0.2}$-TCl	432	453	-6.19	428-480
PM6-$Cl_{0.5}$-*b*-D18-$Cl_{0.5}$-TCl	427	451	-6.33	420-491
PM6-$Cl_{0.2}$-*b*-D18-$Cl_{0.8}$-TCl	428	459	-6.61	415-490
PM6-$Cl_{0.8}$-*b*-D18-$Cl_{0.2}$-BTB	431	450	-6.31	411-488

*(a) The temperature at which the donor material reaches a 5% mass loss;

(b) The temperature at which the donor material reaches its fastest decomposition rate;

(c) The fastest decomposition rate that donor material can achieve;

(d) The range of donor materials in glass transition temperature.

Table S11. Detailed characterization of mechanical properties for pristine and blend films.

Active layer	AFM PFQNM	Film on Water		
	Elastic modulus [GPa]	Crack-onset strain [%]	Stress [(a)] [MPa]	Elastic modulus [(b)] [GPa]
PM6	1.73	8.19	4.00	0.66
PM6-$Cl_{0.8}$-*r*-D18-$Cl_{0.2}$-TCl	1.52	15.19	34.66	4.08
PM6-$Cl_{0.8}$-*b*-D18-$Cl_{0.2}$-TCl	2.21	32.02	36.80	3.38
PM6-$Cl_{0.5}$-*b*-D18-$Cl_{0.5}$-TCl	2.35	22.14	52.39	4.65
PM6-$Cl_{0.2}$-*b*-D18-$Cl_{0.8}$-TCl	1.43	16.99	18.36	4.19
PM6-$Cl_{0.8}$-*b*-D18-$Cl_{0.2}$-BTB	1.87	40.29	57.79	3.59
PM6-$Cl_{0.8}$-*b*-D18-$Cl_{0.2}$-TCl: PM6	(-)	24.14	4.90	0.91
PM6: BTP-eC9	1.67	4.60	7.9	3.58
PM6-$Cl_{0.8}$-*r*-D18-$Cl_{0.2}$-TCl: BTP-eC9	2.41	10.11	43.78	6.85
PM6-$Cl_{0.8}$-*b*-D18-$Cl_{0.2}$-TCl: BTP-eC9	1.74	22.58	54.31	4.08
PM6-$Cl_{0.5}$-*b*-D18-$Cl_{0.5}$-TCl: BTP-eC9	1.76	17.75	54.31	6.11
PM6-$Cl_{0.2}$-*b*-D18-$Cl_{0.8}$-TCl: BTP-eC9	2.38	16.71	43.24	4.69
PM6-$Cl_{0.8}$-*b*-D18-$Cl_{0.2}$-BTB: BTP-eC9	1.46	25.38	43.79	4.07
PM6-$Cl_{0.8}$-*b*-D18-$Cl_{0.2}$-TCl: PM6: BTP-eC9	(-)	11.03	18.33	3.73
PM6-$Cl_{0.8}$-*b*-D18-$Cl_{0.2}$-BTB: PM6: BTP-eC9	(-)	14.99	37.66	4.47
D18: BTP-eC9	(-)	4.95	5.13	3.85
D18: PM6-$Cl_{0.8}$-*b*-D18-$Cl_{0.2}$-TCl: BTP-eC9	(-)	14.49	35.87	4.86
D18: PM6-$Cl_{0.8}$-*b*-D18-$Cl_{0.2}$-BTB: BTP-eC9	(-)	18.84	61.75	4.99
PM6-$Cl_{0.8}$-*b*-D18-$Cl_{0.2}$-TCl: PY-IT	(-)	29.48	71.24	5.26
PM6-$Cl_{0.8}$-*b*-D18-$Cl_{0.2}$-BTB: PY-IT	(-)	36.52	77.45	5.53

*(a) The highest stress value achieved in corresponding films.

(b) Gradient of slope in MCD elastic deformation region.

Table S12. Detailed photoelectric parameters for flexible MCD-based OSCs.

MCD	Acceptor	D/A[(a)]	V_{oc} [V]	J_{sc} [mA cm^{-2}]	*FF* [%]	PCE [%]
PM6-Cl$_{0.8}$-*b*-D18-Cl$_{0.2}$-TCl	**BTP-eC9**	1: 1.2	0.845	27.02	75.40	17.21
PM6-Cl$_{0.8}$-*b*-D18-Cl$_{0.2}$-BTB	**BTP-eC9**	1: 1.2	0.833	26.53	64.99	14.36
PM6-Cl$_{0.8}$-*b*-D18-Cl$_{0.2}$-TCl :PM6	**BTP-eC9**	1: 1.2	0.849	27.84	76.29	18.03

*(a) The total concentration of the donor and NFA-SMA acceptor (BTP-eC9) remained identical with a best ratio of 1:1.2.

References

[1] J. W. Lee , C. Sun, S. Lee, D. J. Kim, E. S. Oh, T. N. L. Phan, T. H. Q. Nguyen, S. Seo, Z. Tan, M. J. Lee, J. Y. Lee, X. Bao, T. S. Kim, C. Lee, Y. H. Kim, B. J. Kim, *Nano Energy* **2024**, 125: 109541.

[2] J. W. Lee, C. Sun, S. W. Lee, G. U. Kim, S. Li, C. Wang, T. S. Kim, Y. H. Kim, B. J. Kim, *Energy Environ. Sci.* **2022**, 15, 4672.

[3] J. W. Lee, S. W. Lee, J. Kim, Y. H. Ha, C. Sun, T. N. L. Phan, S. Lee, C. Wang, T. S. Kim, Y. H. Kim, B. J. Kim, *J. Mater. Chem. A* **2022**, 10, 20312.

[4] J. He, D. Zhang, J. Liu, l. Yang, Y. Gao, M. Shao, *ACS Appl. Mater. Interfaces* **2024**, 16, 17, 22294.

[5] C. Sun, J. W. Lee, Z. Tan, T. N. L. Phan, D. Han, H. G. Lee, S. Lee, S. K. Kwon, B. J. Kim, Y. H. Kim, *Adv. Energy Mater.* **2023**, 13, 2301283.

[6] S. Seo, J. W. Lee, D. J. Kim, D. Lee, T. N. L. Phan, J. Park, Z. Tan, S. Cho, T. S. Kim, B. J. Kim, *Adv. Mater.* **2023**, 35, 2300230.

[7] J. W. Lee, S. Seo, S. W. Lee, G. U. Kim, S. Han, T. N. L. Phan, S. Lee, S. Li, T. S. Kim, J. Y. Lee, B. J. Kim, *Adv. Mater.* **2022**, 34, 2207544.

[8] J. W. Lee, C. Lim, S. W. Lee, Y. Jeon, S. Lee, T. S. Kim, J. Y. Lee, B. J. Kim, *Adv. Energy Mater.* **2022**, 12, 2202224.

[9] J. W. Lee, C. Sun, J. Lee, D. J. Kim, W. J. Kang, S. Lee, D. Kim, J. Park, T. N. L. Phan, Z. Tan, F. S. Kim, J. Y. Lee, X. Bao, T. S. Kim, Y. H. Kim, B. J. Kim, *Adv. Energy Mater.* **2024**, 14, 2303872.

[10] J. W. Lee, H. G. Lee, E. S. Oh, S. W. Lee, T. N. L. Phan, S. Li, T. S. Kim, B. J. Kim, *Joule*, **2024**, 8, 204.

[11] Z. Genene, J. W. Lee, S. W. Lee, Q. Chen, Z. Tan, B. A. Abdulahi, D. Yu, T. S. Kim, B. J. Kim, E. Wang, *Adv. Mater.* **2022**, 34, 2107361.

[12] C. Lin, R. Peng, W. Song, Z. Chen, T. Feng, D. Sun, Y. Bai, Z. Ge, *Angew. Chem., Int. Ed.* **2024**, 63, e202407040.

[13] W. Feng, Z. Lin, J. Cui, W. Lv, W. Wang, Q. Ling, *Sol. Energy Mater. Sol. Cells* **2019**, 200, 109982.

[14] G. Zhang, Y. Fu, L. Qiu, Z. Xie, *Polymer* **2012**, 53, 4407.

[15] M. Wu, L. Shi, Y. Hu, L. Chen, T. Hu, Y. Zhang, Z. Yuan, Y. Chen, *Chin. Chem. Lett.* **2019**, 30, 1161.

[16] Y. Huang, M. Zhang, H. Chen, F. Wu, Z. Cao, L. Zhang, S. Tan, J. Mater. Chem. A **2014**, 2, 5218.

[17] M. C. Yuan, M. Y. Chiu, C. M. Chiang, K. H. Wei, *Macromolecules* **2010**, 43, 6270.

[18] P. Shen, H. Bin, L. Xiao, Y. Li, *Macromolecules* **2013**, 46, 9575.

[19] H. Jung, G. Yu, S. Jang, I. Hwang, B. Kim, B. S. Kim, Y. Lee, *Org. Electron.* **2020**, 86, 105929.

[20] Z. Li, X. Wang, J. Ren, G. Gan, C. Liu, Q. Sun, H. Wang, Y. Hao, *J. Mater. Chem. C* **2018**, 6, 4555.

[21] D. Kotowski, S. Luzzati, G. Bianchi, A. Calabrese, A. Pellegrino, R. Po, G. Schimperna, A. Tacca, *J. Mater. Chem.* A **2013**, 1, 10736.

[22] X. Xu, G. Zhang, Y. Zhao, J. Liu, Y. Li, Q. Peng, *Chin. J. Polym. Sci.* **2017**, 35, 249.

[23] S. M. Bang, S. Kang, Y. S. Lee, B. Lim, H. Heo, J. Lee, Y. Lee, S. Na, *RSC Adv.* **2017**, 7, 1975.

[24] S. H. Kang, T. Kumari, S. M. Lee, M. Jeong, C. Yang, *Adv. Energy Mater.* **2017**, 7, 1700349.

[25] K. Li, Z. Hu, Z. Zeng, Z. Huang, W. Zhong, L. Ying, F. Huang, *Org. Electron.* **2018**, 57, 317.

[26] M. L. Keshtov, S. A. Kuklin, I. O. Konstantinov, I. E. Ostapov, D. Y. Godovsky, E. E. Makhaeva, Z. Xie, G. D. Sharma, *J. Polym. Sci., Part A: Polym. Chem.* **2019**, 57, 1478.

[27] T. Kim, J. Y. Lee, J. Heo, B. Lim, J. Y. Kim, *Polym. Chem.* **2018**, 9, 1216.

[28] M. L. Keshtov, S. A. Kuklin, I. O. Konstantinov, I. E. Ostapov, E. E. Makhaeva,

A. Y. Nikolaev, Z. Xie, Y. Zou, G. D. Sharma, *New J. Chem.* **2019**, 43, 5325.

[29] M. H. Hoang, G. E. Park, D. L. Phan, T. T. Ngo, T. V. Nguyen, S. H. Park, M. J. Cho, D. H. Choi, *J. Polym. Sci., Part A: Polym. Chem.* **2018**, 56, 1528.

[30] X. Wang, K. Dou, B. Shahid, Z. Liu, Y. Li, M. Sun, N. Zheng, X. Bao, R. Yang, *Chem. Mater.* **2019**, 31, 6163.

[31] X. Jing, Y. Zhong, Q. Wang, F. Li, X. Wang, K. Zhang, M. Sun, *Polym. Int.* **2021**, 70, 443.

[32] D. H. Kim, T. T. T. Bui, S. Rasool, C. E. Song, H. K. Lee, S. K. Lee, J. C. Lee, W. W. So, W. S. Shin, *ACS Appl. Mater. Interfaces* **2018**, 11, 2189.

[33] T. Dai, A. Tang, Z. He, M. Du, P. Lei, Q. Zeng, Z. Wang, Y. Wang, S. Lu, Y. Zhong, E. Zhou, *Energy Environ. Sci.* **2023**, 16, 2199.

[34] J. Ji, J. Xie, J. Tang, K. Zheng, Z. Liang, Sol. RRL **2021**, 5, 2100142.

[35] X. Huang, L. Zhang, Y. Cheng, J. Oh, C. Li, B. Huang, L. Zhao, J. Deng, Y. Zhang, Z. Liu, F. Wu, X. Hu, C. Yang, L. Chen, Y. Chen, *Adv. Funct. Mater.* **2022**, 32, 2108634.

[36] M. Pu, H. Chen, P. Chao, Y. Zhu, N. Zheng, H. Lai, T. Zhao, F. He, *ACS Appl. Polym. Mater.* **2020**, 3, 14.

[37] H. W. Cho, S. Y. Jeong, Z. Wu, H. Lim, W. W. Park, W. Lee, J. V. S. Krishna, O. H. Kwon, J. Y. Kim, H. Y. Woo, *J. Mater. Chem. A* **2023**, 11, 7053.

[38] J. Wu, G. Li, J. Fang, X. Guo, L. Zhu, B. Guo, Y. Wang, G. Zhang, L. Arunagiri, F. Liu, H. Yan, M. Zhang, Y. Li, *Nat. Commun.* **2020**, 11, 1.

[39] X. Guo, Q. Fan, J. Wu, G. Li, Z. Peng, W. Su, J. Lin, L. Hou, Y. Qin, H. Ade, L. Ye, M. Zhang, Y. Li, Angew. Chem. **2021**, 133, 2352.

[40] Y. Zhang, J. Deng, Q. Mao, S. Y. Jeong, X. Huang, L. Zhang, B. Lee, B. Huang, H. Y. Woo, C. Yang, J. Xu, F. Wu, Q. Y. Cao, L. Chen, *Chem. Eng. J.* **2023**, 457, 141343.

[41] H. R. Bai, Q. An, H. F. Zhi, M. Jiang, A. Mahmood, L. Yan, M. Q. Liu, Y. Q. Liu, Y. Wang, J. L. Wang, *ACS Energy Lett.* **2022**, 7, 3045.

[42] X. Chen, C. Liao, M. Deng, X. Xu, L. Yu, R. Li, Q. Peng, *Chem. Eng. J.* **2023**, 451. 139046.

[43] B. Zheng, Y. Yue, J. Ni, R. Sun, J. Min, J. Wang, L. Jiang, L. Huo, *Sci. China: Chem.* **2022**, 65, 964.

[44] J. Wang, M. Zhang, J. Lin, Z. Zheng, L. Zhu, P. Bi, H. Liang, X. Guo, J. Wu, Y. Wang, L. Yu, J. Li, J. Lv, X. Liu, F. Liu, J. Hou, Y. Li, *Energy Environ. Sci.* **2022**, 15, 1585.